

# We are IntechOpen, the world's leading publisher of Open Access books Built by scientists, for scientists

6,300

Open access books available

171,000

International authors and editors

190M

Downloads

Our authors are among the

154

Countries delivered to

TOP 1%

most cited scientists

12.2%

Contributors from top 500 universities



WEB OF SCIENCE™

Selection of our books indexed in the Book Citation Index  
in Web of Science™ Core Collection (BKCI)

Interested in publishing with us?  
Contact [book.department@intechopen.com](mailto:book.department@intechopen.com)

Numbers displayed above are based on latest data collected.  
For more information visit [www.intechopen.com](http://www.intechopen.com)



# Waveguide Amplifier for Extended Reach of WDM/FSO

*Bentahar Attaouia, Kandouci Malika, Ghouali Samir  
and Dinar Amina Elbatoul*

## Abstract

In this chapter, EYDWA (erbium ytterbium doped waveguide amplifier) is characterized for wavelength division multiplexing (WDM) approach on free space optical (FSO) transmission systems with channels being spaced at 0.4 nm interval. Moreover, in this paper, was study different characterizations of EYDWA amplifier, which depend essentially on the opt-geometric parameters, such as concentrations of ions erbium, length of the waveguide and the effect of those parameters to optimize the performance of proposed system. Furthermore, the results reveal that the EYDWA booster (post-amplification) can improve the high performance remarkably under clear rain and the acceptable transmission can be carried out up to 26 km while it get reduced to 19.5 km by using pre-amplification.

**Keywords:** free space optical, BER, EDWA, WDM, atmospheric condition

## 1. Introduction

FSO (free space optics) is an optical communication technology in which contains three components: transmitter, free space transmitted, and receiver. The transmitter requires light, which can be focused by using either light emitting diode (LED) or laser (light amplification by stimulated emission of radiation) to transmit information through the atmosphere. At the receiver, a photodiode converts the optical intensity signal back into an electrical signal and the information is recovered [1, 2].

The FSO communication system has the advantages of unrestricted spectrum and high-speed transmission over other wireless communication systems. This system is likely to replace other wireless communication systems in many fields and become the solution for last-mile communication. The main limitation of FSO is seen in worse weather conditions where it suffers highest attenuation [3].

Optical network that apply wavelength division multiplexing (WDM) is currently widely used in existing telecommunications infrastructures and is expected to play a significant role in FSO system supporting a large variety of services having very different requirements in terms of bandwidth capacity which ensures multiservice and multicasting opportunity [4, 5].

WDM FSO systems use a single light beam to transmit the multiplexed signal through free space [6]. A multiplexer is used at the transmitter to combine different modulated carriers and a demultiplexer at the receiver to restore each one (Figure 1).

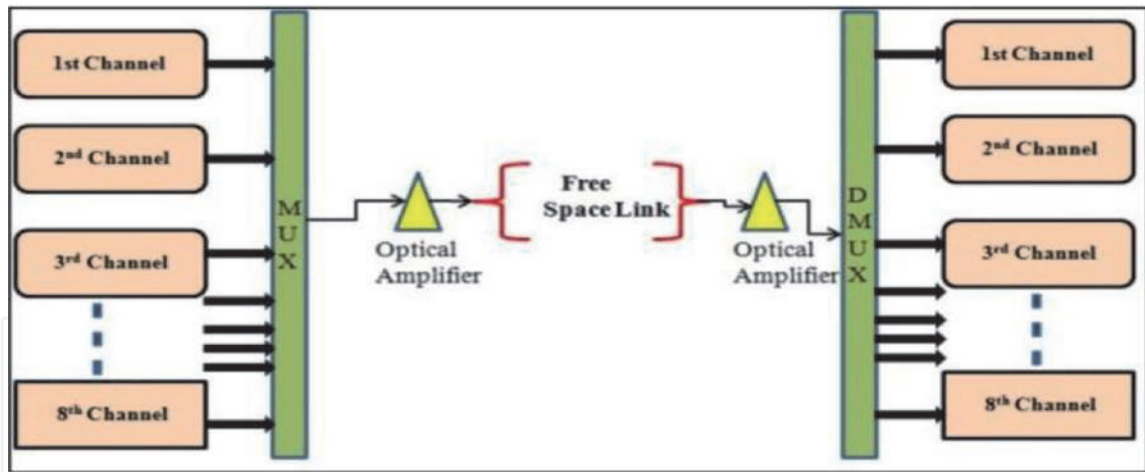


Figure 1.  
The system setup of WDM-FSO.

## 2. Optical amplifier

An optical amplifier is a device that amplifies an optical signal directly, without the need to first convert it to an electrical signal. In the 1990's, optical amplifiers, which directly amplified the transmission signal, became widespread minimizing system intricacies and cost [7]. Many techniques have been proposed to improve the performance of FSO link like the amplification of signal [3].

To maintain the integrity of information sent from one location to another, optical amplifiers, such as doped fiber amplifiers (DFA), doped waveguide amplifiers (DWA), and semiconductor optical amplifiers (SOA), are utilized to extend transmission range for the cost-effective implementation of FSO and can be used for amplification of WDM network easily [4].

### 2.1 Doped fiber amplifiers

Doped fiber amplifiers (DFAs) are optical amplifiers that use a doped optical fiber as a gain medium to amplify an optical signal [8]. They are related to fiber lasers. The signal to be amplified and a pump laser are multiplexed into the doped fiber, and the signal is amplified through interaction with the doping ions.  $\text{Er}^{3+}$  is one of the most commonly used doped ions in integrated photonics and the EDFA is one effective way to amplify light signal at optical communication window between 1500 to 1600 nm.

#### 2.1.1 Erbium doped fiber amplifier

The erbium-doped fiber amplifier (EDFA) is the most deployed fiber amplifier as its amplification window coincides with the third transmission window of silica-based optical fiber and has demonstrated high gain, low noise, and full compatibility with DWDM signals. In general, EDFA works on the principle of stimulating the emission of photons. With EDFA, an erbium-doped optical fiber at the core is pumped with a laser at or near wavelengths of 980 nm and 1480 nm, and gain is exhibited in the 1550 nm region (**Figure 2**).

### 2.2 Doped waveguide amplifier

Waveguide amplifiers, in particular, are new integrated optical products well suited to metro/access applications. Some of the intrinsic benefits for using this later

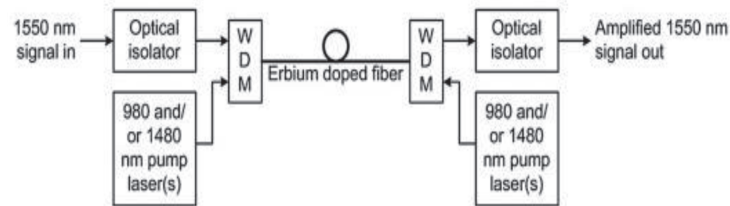


**Figure 2.**  
 Erbium doped fiber amplifier block diagram.

include their compactness, performance, flexibility, and lower-cost processing [9]. These integrated devices offer the prospect of combining passive and active components on the same substrate while producing compact and robust devices at lower cost than commercially available fiber-based counterpart. However, the way to implement all-optical network relies on the control of gain variation of amplifiers which is sensitive to total input power variation [1, 8].

### 2.2.1 Erbium-doped waveguide amplifier

The erbium-doped waveguide amplifier (EDWA) are planar waveguides doped with erbium ions and are excited similar to EDFAs. EDWAs integrate several functions and components onto a mass produced integrated circuit and have recently received considerable attention as a potential high-gain medium for optical amplification in the communication band (**Figure 3**) [8, 9].

## 3. Concentration quenching of erbium

EDWAs are less efficient than EDFAs due to higher erbium concentration in the waveguide on the substrate. Greater erbium ion concentration causes more pumping power to quench to the system. Additionally, there is greater loss in waveguides than fibers. Concentration quenching is the reduction in quantum efficiency of a erbium ion as its concentration increases. It generally manifests itself by a shortening of the measured metastable level lifetime and occurs mostly through cross relaxation or co-operative up-conversion processes.

When the concentration levels are such that the separation between two erbium ions is greater than the diameter of an individual erbium ion then the up conversion process is called “homogeneous up conversion (HUC)”. In addition to the above-mentioned effects, another important effect that needs to be investigated is the pair induced quenching (PIQ). This later is an inhomogeneous phenomenon

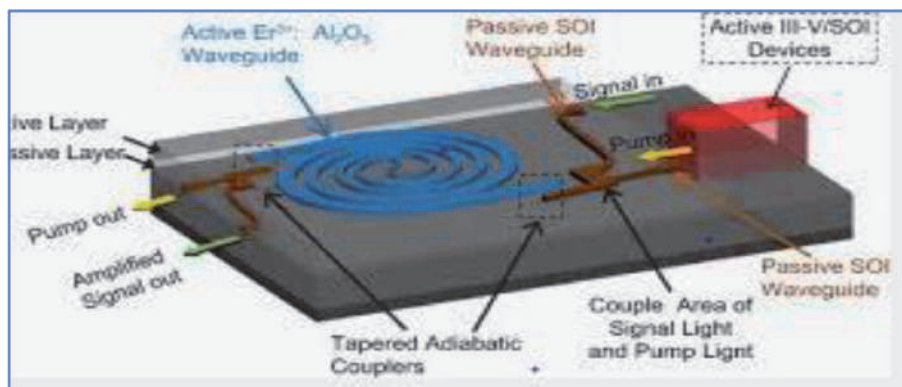


**Figure 3.**  
 Erbium-doped waveguide amplifiers block diagram.

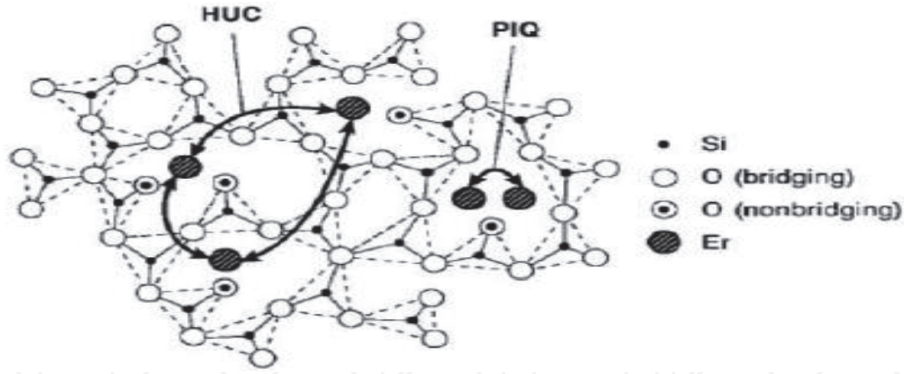


**Figure 4.** Scheme of pair-induced quenching (PIQ) and up-conversion (HUC) processes in erbium-doped fiber amplifier.

caused by clustered ions when the  $\text{Er}^{+3}$  the inter-ionic distance between two erbium ions becomes less and they come much closer to each other so as to form “clusters” [10]. This issue has been addressed by co-doping the erbium by ytterbium ( $\text{Yb}^{+3}$ ) (Figure 4).

#### 4. Co doping with ytterbium ions to inhibit PIQ

To increase the absorption cross section, ytterbium ions ( $\text{Yb}^{3+}$ ) are usually co-doped as a sensitizer. The introduction of ytterbium can effectively restrain the erbium  $\text{Er}^{3+}$  ion clusters, and reduce up-conversion nonlinear side effect. This can increase the total gain and the unit length gain greatly [11].

The performance of the  $\text{Er}^{3+} - \text{Yb}^{3+}$  co-doped waveguide amplifiers (EYDWA) is better than that of the EDWA, and the EYDWAs are therefore expected to be an attractive high-gain medium material for optical amplification because of their use as amplifiers in optical telecommunications and as compact light sources for eye-safe range finding in the  $1.55 \mu\text{m}$  spectral range (Figure 5) [12, 13].

Ytterbium offers the advantage of a high absorption cross-section and a good spectral overlap of its emission with erbium  $4 I_{11/2}$  absorption, leading to an efficient energy transfer from ytterbium to erbium.

The rate equations for  $\text{Er}^{+3}$  and  $\text{Yb}^{+3}$  population can be written as [14]:

$$\frac{dN_2}{dt} = -A_{21}N_2 - 2U_{up} N_2^2 + N_1\sigma_{sa}\phi_s - N_2\sigma_{se}\phi_s + \gamma_{32}N_3 \quad (1)$$

$$\frac{dN_3}{dt} = -N_3\sigma_{pe}\phi_p + N_1\sigma_{pa}\phi_p + PN_1N_6 - P'N_3N_5 - N_3\sigma_{32} + \gamma_{43}N_4 \quad (2)$$

$$\frac{dN_4}{dt} = C_{up}N_2^2 - \gamma_{43}N_4 \quad (3)$$

$$\sum_i^4 N = N_{Er} \quad (4)$$

$$\frac{dN_3}{dt} = PN_1N_6 - P'N_3N_5 - N_5\sigma'_{pa}\phi_p + N_6\sigma'_{pa}\phi_p + N_6\sigma'_{pe}\phi_p + A_{65}N_6\gamma_{43}N_4 \quad (5)$$

$$N_{Yb} = N_5 + N_6 \quad (6)$$

where,  $N_1$ ,  $N_2$ ,  $N_3$  and  $N_4$  are the Er population densities ( $\text{m}^{-3}$ ) of  $4I_{15/2}$ ,  $4I_{13/2}$ ,  $4I_{11/2}$ ,  $4I_{9/2}$  levels, respectively. The quantities  $N_5$ ,  $N_6$  are the  $\text{Yb}^{+3}$  population

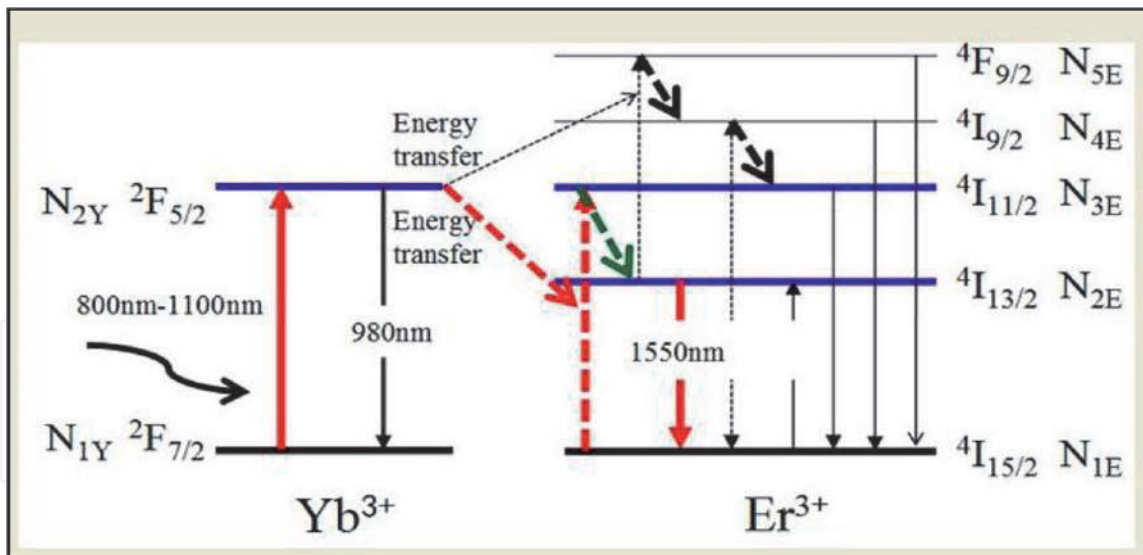


**Figure 5.**  
 Energy level diagram of erbium and ytterbium system.

densities ( $m^{-3}$ ) of the  $2F_{7/2}$  and  $2F_{5/2}$  levels respectively. Whereas,  $\varphi_p$ ,  $\varphi_s$ ,  $\sigma'_{pa}$ ,  $\sigma'_{pe}$ ,  $A_{21}$ ,  $A_{65}$ ,  $P$ ,  $P'$ ,  $C_{up}$  are defined in **Table 1**.

The spontaneous emission rates of  $Er^{+3}$  and  $Yb^{+3}$  can be calculated by:

$$\sigma_a = \frac{h\gamma n}{C} B_{12} g_{12}(\gamma), \sigma_e = \frac{h\gamma n}{C} B_{21} g_{21}(\gamma) \quad (7)$$

where  $g_{12}(\gamma)$  and  $g_{21}(\gamma)$  are the normalized emission and absorption line shape respectively,  $n$  is the refractive index of the medium and  $B_{12}$  and  $B_{21}$  are the coefficients of transition. Then the signal gain  $G$  and total noise Figure  $NF$  are given by:

$$G = \exp \left[ \int_0^L g(z) dz \right],$$

$$NF = 10 \log \log_{10} \left[ \frac{1}{G} + \frac{P_{ASE}}{G h \gamma B_0} - \frac{P_{SSE}}{h \gamma B_0} \right] \quad (8)$$

Parameter	Definition
$\varphi_p$	The pump photon flux
$\varphi_s$	The signal photon flux
$\sigma_{pe}$	The stimulated emission cross section for $Er^{+3}$
$\sigma_{pa}$	The absorption cross section for $Er^{+3}$
$\sigma'_{pe}$	The stimulated emission cross section for $Yb^{+3}$
$\sigma'_{pa}$	The absorption cross section for $Yb^{+3}$
$A_{21}$	The spontaneous emission rate of $Er^{+3}$
$A_{65}$	The spontaneous emission rate $Yb^{+3}$
$K$ and $K'$	The coefficient of energy transfer for the concentrations of $E^{+3}$ and $Yb^{+3}$
$C_{up}$	The up conversion coefficient

**Table 1.**  
 Parameter definition for equations.

where  $\gamma$  is the signal frequency,  $B_o$  is the noise bandwidth,  $P_{ASE}$  and  $P_{SSE}$  are the power of amplified spontaneous emission, and the power of source spontaneous emission, respectively.

## 5. Comparison of EDFA and EYDWA for WDM/FSO network

The FSO-WDM with eight input signals using EYDWA amplifier as a pre- or post-TT6Af an externally modulated WDM transmitter generating eight NRZ signals at 2.5 Gbit/s with input power of  $-10$  dBm, the eight channels are multiplexed with a spacing set at 0.8 nm in the wavelength range 1550 to 1554.8 nm. Then the signal is ready to travel through 30 Km range of FSO. On the receiver's side, the avalanche photodiode (APD) is used followed by a low pass filter and a 3R regenerator. The performance is analyzed using BER analyzer which gives the related BER, power level and eye diagrams.

**Figures 6** and 7 shows the dependence of the gain and noise figure on frequency for both optical amplifiers EDFA and EYDWA, respectively. It is evident that the EYDWA amplifier also offers a better price/performance ratio (better gain of 32 dB and high NF of 11 dB) than comparable EDFA amplifier (Gain of 15 dB and better N Fof 5 dB) for WDM/FSO network applications. Most of the intrinsic advantages of EYDWAs come from their ability to provide high gain in very short optical paths than EDFA amplifier. This capability gives vendors more flexibility in the design of a compact amplifier.

### 5.1 Concentration quenching affects

The homogeneous up conversion tends to cause more impairment in the EDFA amplifier performance than in the EYDWA amplifier. **Figure 8** shows variation of gain as a function of the HUC coefficient [15]. It is observed that as this later increased; the gain spectrum decreased and showed larger variation especially for EDFA as compared as EYDWA amplifier. Furthermore for UHC coefficient higher of  $2.10^{-22} \text{ m}^3/\text{s}$  we can notice lowest results in term of gain for EDFA, however EYDWA amplifier provides the best results (high and flat gain). Also the maximum

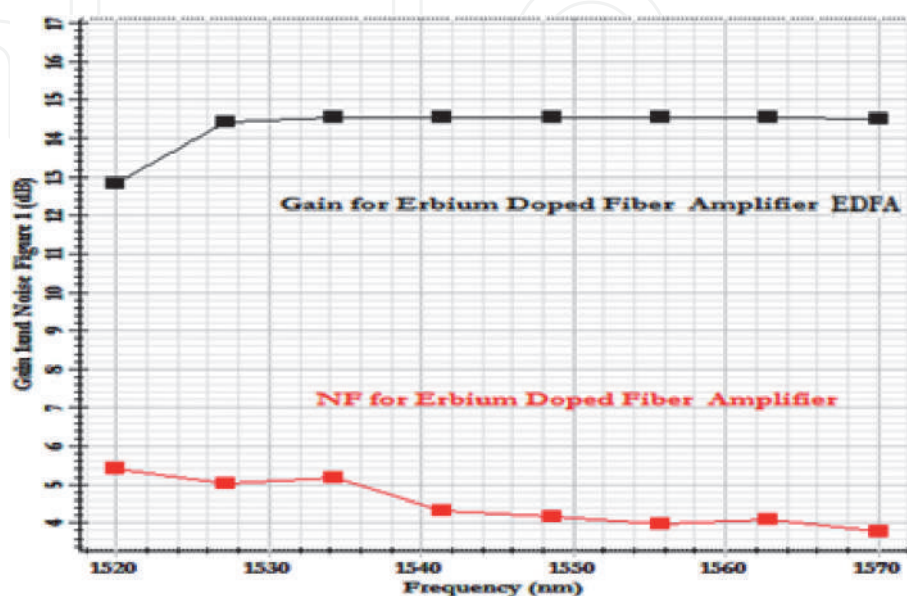


**Figure 6.** Gain and noise figure as a function of frequency for the erbium doped fiber amplifier (EDFA).

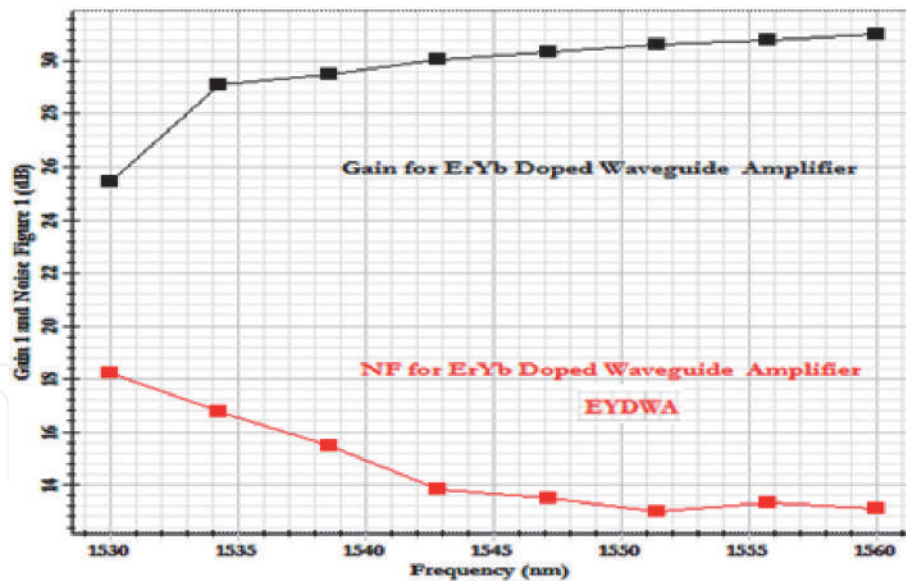


Figure 7.  
 Gain and noise figure as a function of frequency for the Er-Yb doped waveguide amplifier (EYDWA).

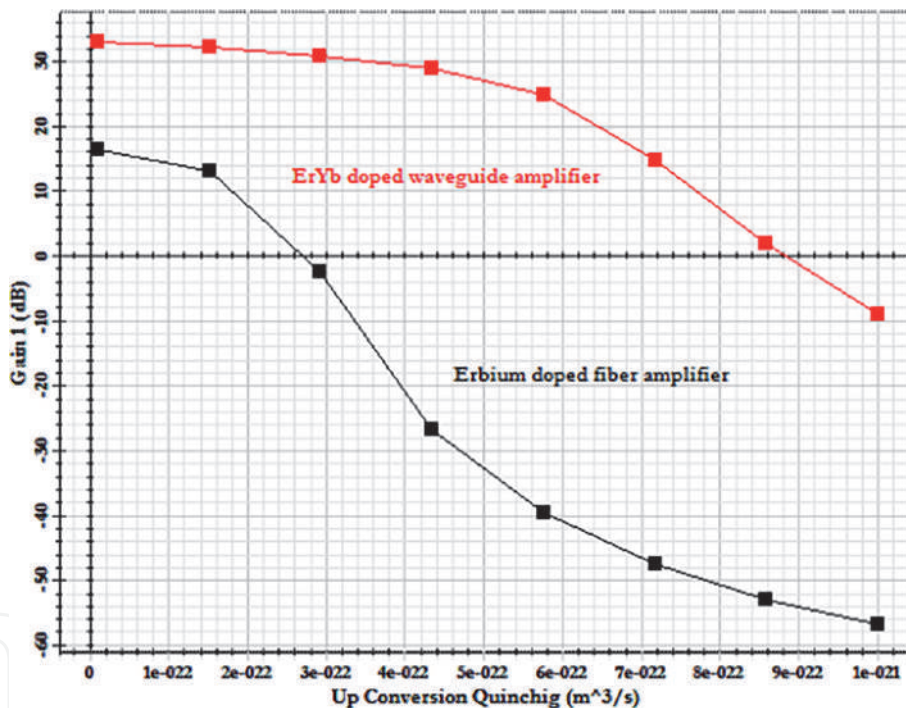


Figure 8.  
 Gain as a function of up-conversion coefficient for the EYDWA and EDFA.

Q factor values occur for EYDWA amplifier and at lower HUC coefficient as compared as EDFA amplifier **Figure 9**.

## 5.2 Influence of length and erbium doping

The critical turning point in the EYDWA technology is finding a compromise between the high erbium ytterbium co-doping levels, which helps create large gain in a short optical length [13]. The dependence of EYDWA performance on the length and erbium ion concentration is studied **Figures 10** and **11**.

For better performance the optimization has been done and it was reported of the system amplified (WDM- FSO) under medium rain and at 2.5 Gbit/s. The EYDWA

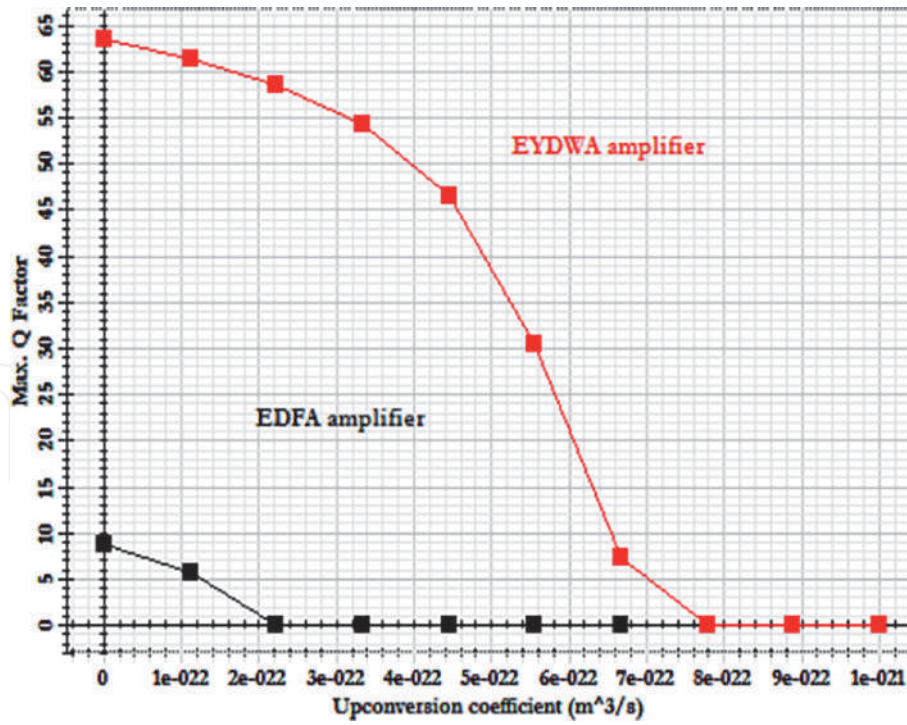


Figure 9. Q factor as a function of up-conversion coefficient for the EYDWA and EDFA.

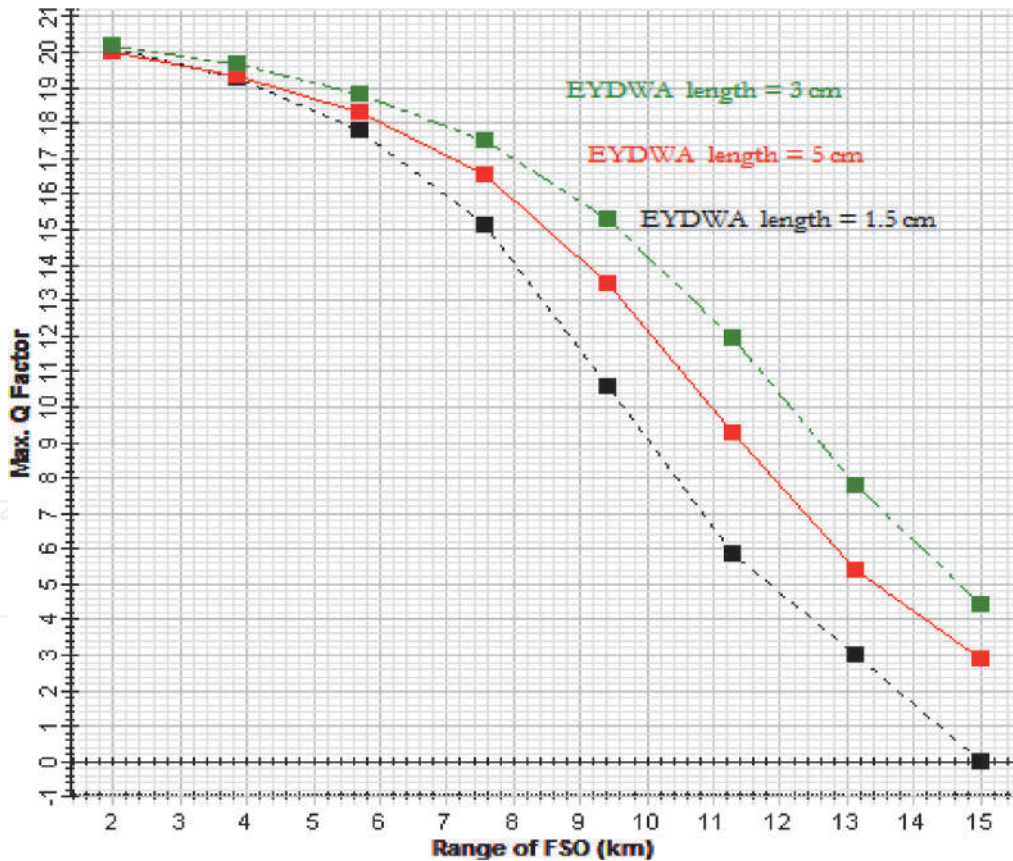


Figure 10. Curves of Q factor versus EYDWA length for WDM-FSO system under medium rain.

amplifier can be reached higher FSO range (over 12 km) with acceptable quality factor (Q values of 6 and BER =  $10^{-9}$ ) by increasing the erbium concentration (up to  $6.10^{26}$  ions/m<sup>3</sup>) and with optimum waveguide length (over 3.5 cm). These results proved that we can achieve high gain with a short device length.

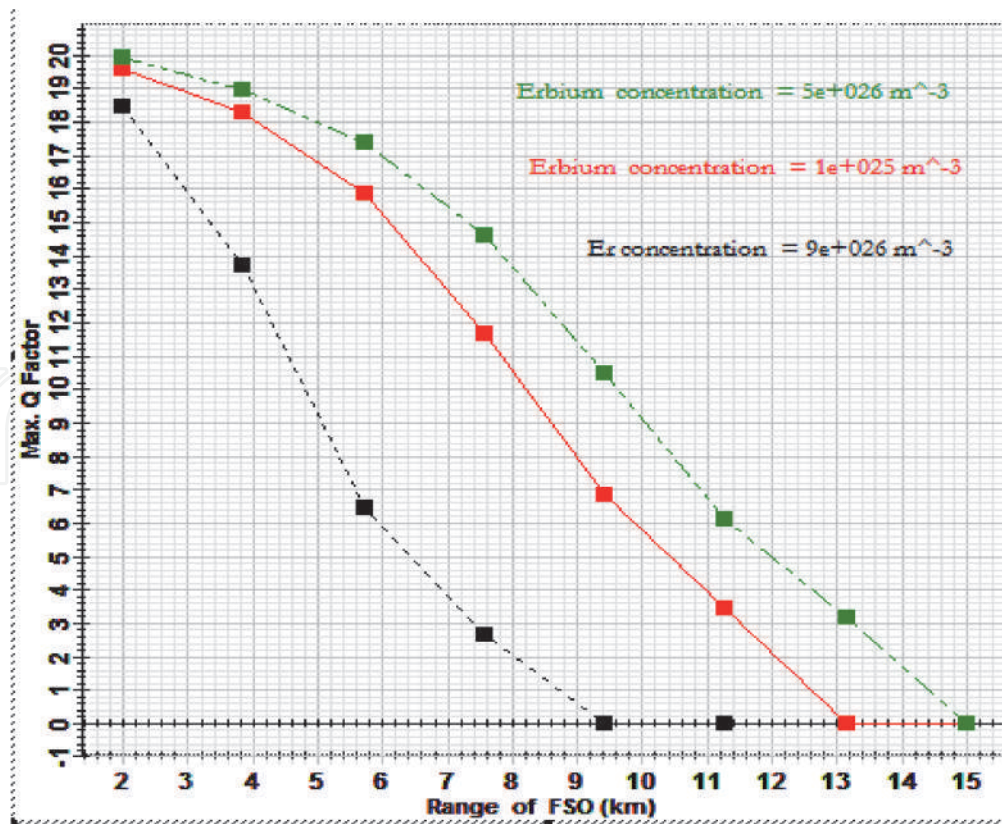


Figure 11. Curves of maximum gain versus erbium ion concentration for WDM- FSO system under medium rain.

### 5.3 Influence of the position of EYDWA amplifier

The performance analysis of the system amplified under clear, medium and heavy rain conditions are shown in “Table 2”, and Max Q factor has been analyzed Figures 12 and 13. It can be seen that under optimized conditions of data rate, the increase in the attenuation (respective intensity of rain) causes the decrease in the maximum transmission distance (FSO range) with acceptable quality factor Q values around of 6.

We note that EYDWA as post-amplifier can be carried the link range up to 26 km at and 8 km at BER  $10^{-9}$  under clear and heavy rain, respectively. However EYDWA preamplifier limits this distance of FSO range to 16 Km and 4.5 km at BER  $10^{-9}$  under clear and heavy rain conditions, respectively.

## 6. Gain flatness of EDFA for a WDM FSO system

An amplifier does not have a flat gain curve, that is, it does not generally provide equal amplification for all wavelengths of signals transmitted over the same

Intensity of rain	System with EYDWA post-amplifier			System with EYDWA pre-amplifier		
	Q factor	BER	Range (Km)	Q factor	BER	Range (Km)
Light (clear) 3 dB	5.8	$10^{-9}$	27	6.12	$10^{-9}$	16
Medium 9 dB	6	$10^{-9}$	12	6.03	$10^{-9}$	8
Heavy 20 dB	6	$10^{-9}$	8	6	$10^{-9}$	4.5

Table 2. Comparison of EYDWA post- and pre-amplifier.

Max. Q Factor (Range (km) ) for EYDWA post amplifier

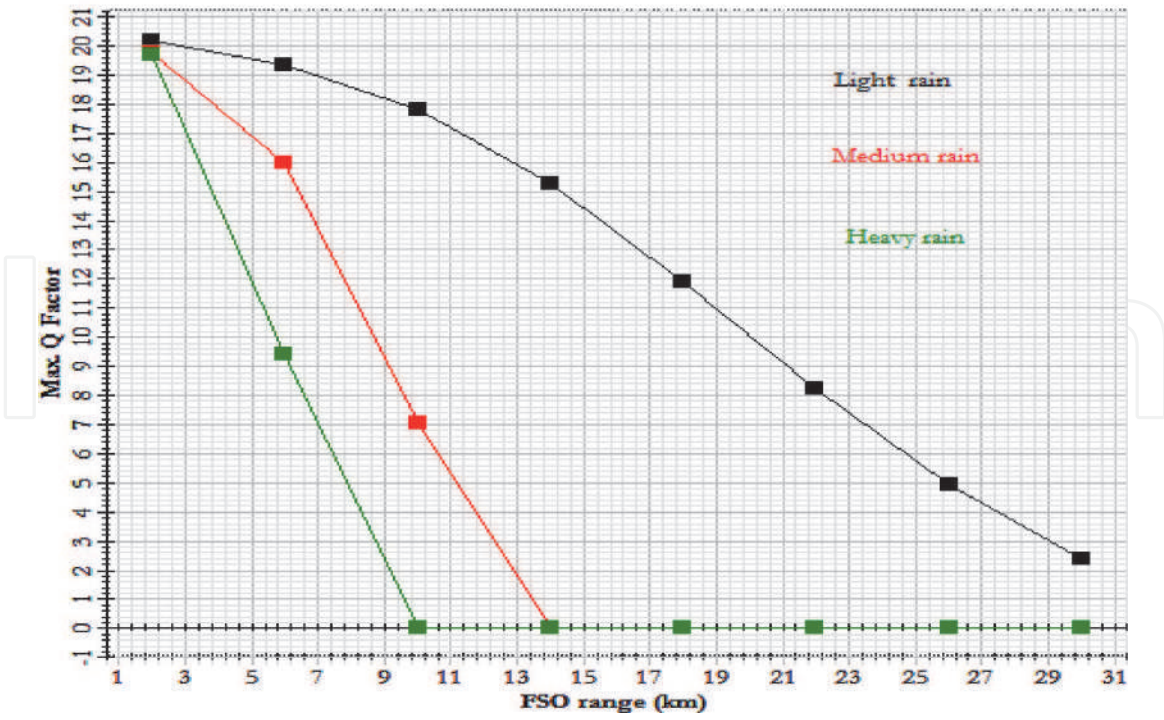


Figure 12. Quality factor as a function of FSO range for EYDWA post- amplifier under clear (light), medium and heavy rain.

Max. Q Factor (Range (km) ) for EYDWA pres-amplifier

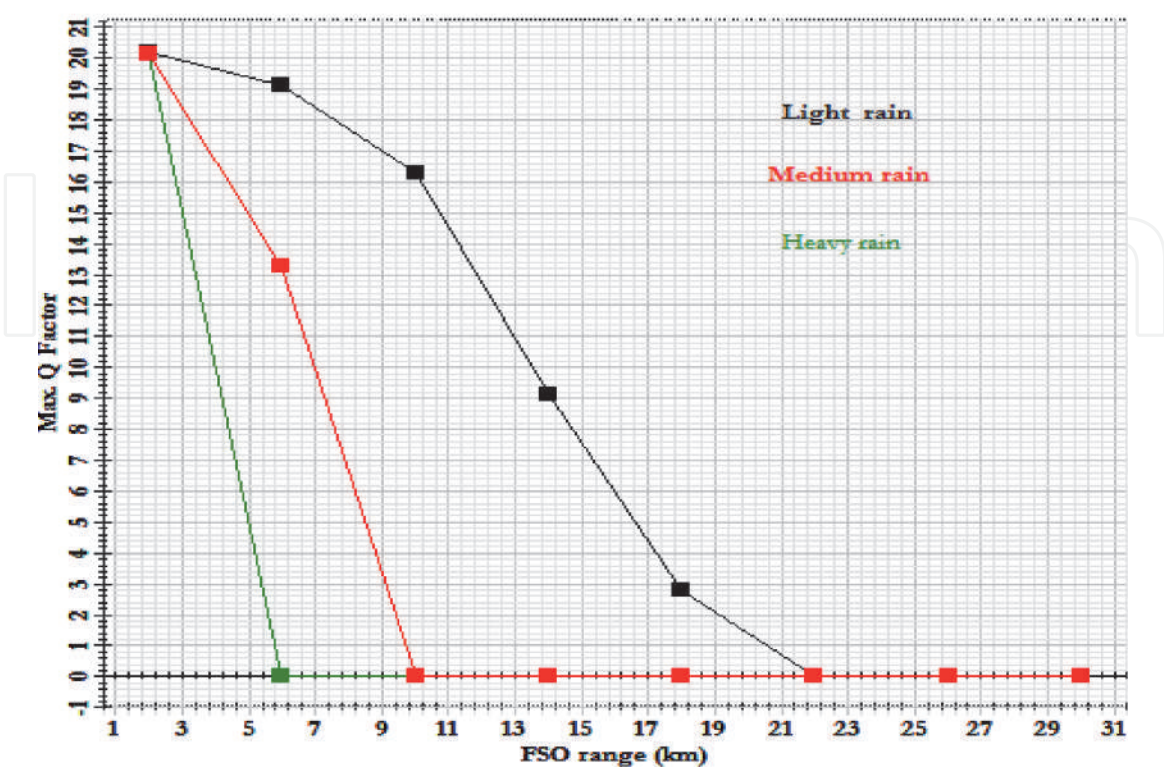


Figure 13. Quality factor as a function of FSO range for EYDWA preamplifier under clear (light), heavy and medium rain.

transmission line (WDM). This disparity is an important limitation for wavelength division multiplexed systems. Good gain flatness requires continuous control of the input power to adjust it to its optimum value [15]. There are several methods for the design of a flat spectral EDFA gain e.g. by combining in-line amplifiers with gain equalizing filters or by controlling some internal EDFA parameters such as the length of the doped fiber, the concentration and the pump power [16].

### 6.1 Equalization of gain with optimization of EDFA parameters

The figures below show the power and noise spectrum as a function of wavelength at the output of the EDFA for different concentrations of erbium ions (from  $1.10^{+24}/m^{-3}$  to  $1.10^{+25}/m^{-3}$ ) and different lengths of the doped fiber (from 2.5 m to 12.5 m), eye diagrams of the simulated system are also shown. According to the graphs obtained, the gray wave represents the noise that decreases as the length and concentration of the doped fiber decreases, while the red symbol in the graphs indicates the sample wavelength (eight wavelengths).

The results obtained show that the concentration of  $5.5 \cdot 10^{+24}/m^{-3}$  and the length of the doped fiber of 7.5 m give the best results in terms of maximum gain (around 26.63 dB) and equalization of the amplified optical spectrum.

It is noticeable that the eye aperture is well open which the quality factor is between 9 and 10 which are higher than 6 that mean that the system works correctly. The BER is higher than  $10^{-12}$  which expresses that the transmission is error-free (Figures 14–18).

The table below summarizes the simulation results at the output of the WDM analyzer for different values of the erbium ion concentration and the length of the doped fiber, where the term  $R_G$  represents the difference between the maximum and minimum value of the EDFA gain (maximum ratio), while  $R_{NF}$  indicates the variation of the noise figure.

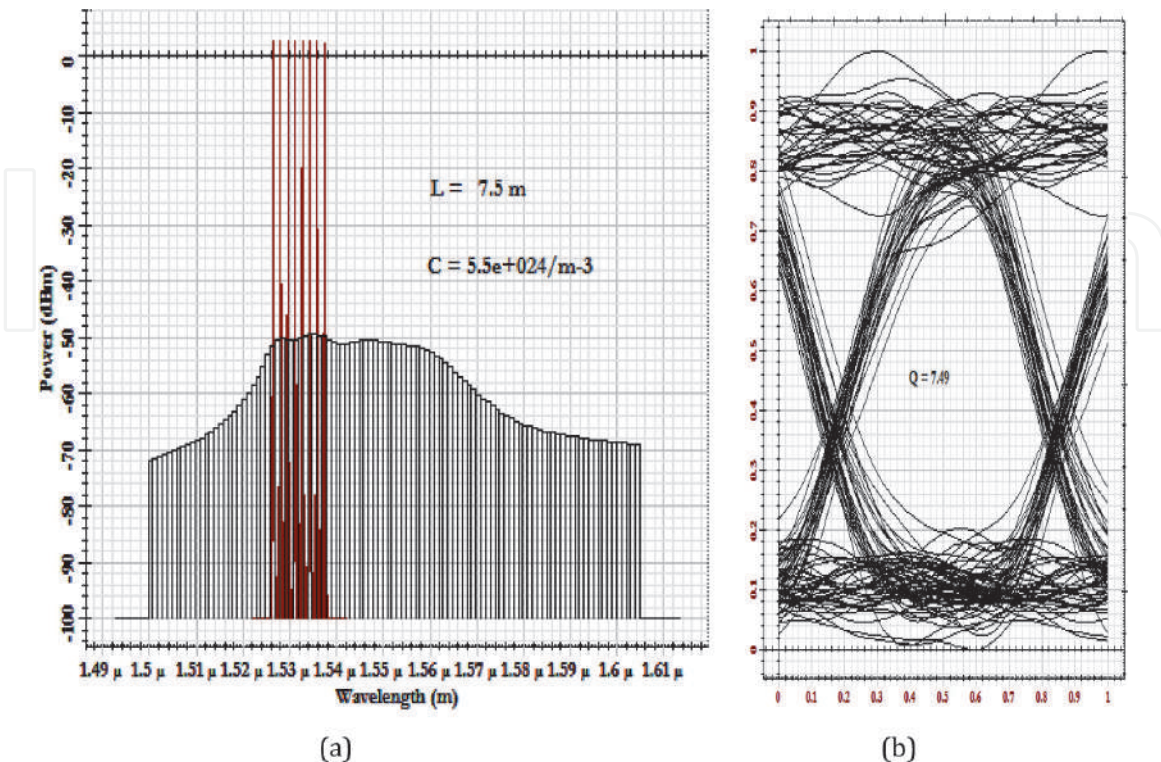


**Figure 14.** (a) Power spectrum and noise figure, (b) eye diagram for concentration and length of the doped fiber ( $C = 5.10^{+24}/m^{-3}$  and  $L = 7, 5 m$ ).

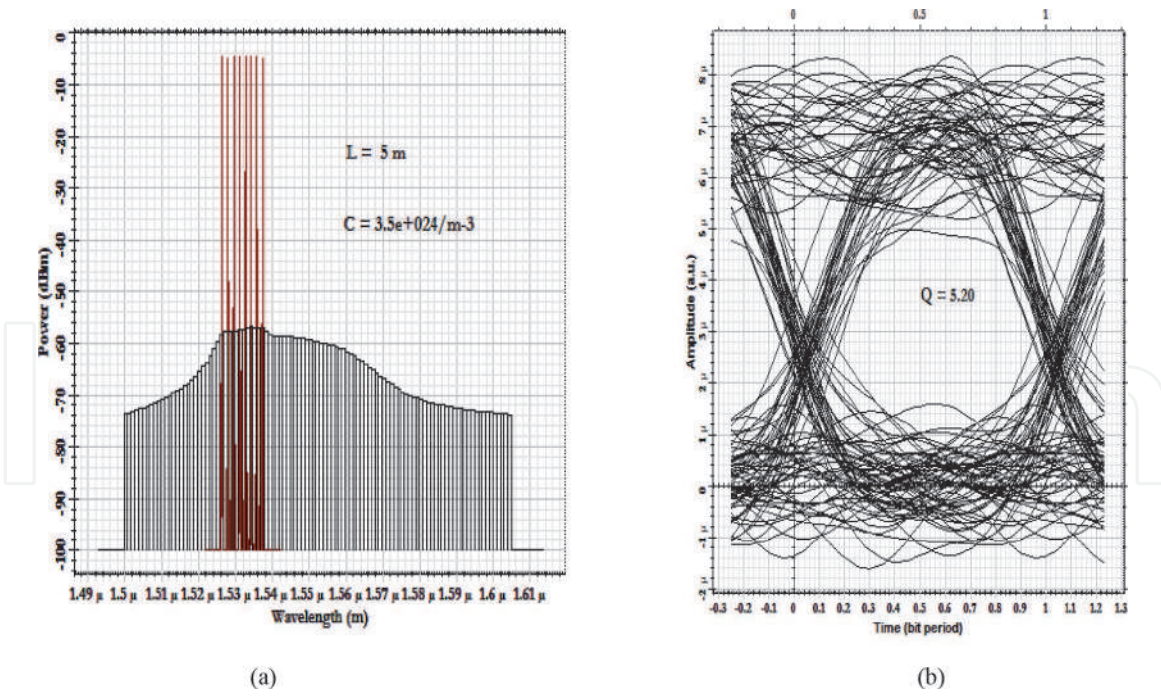


Figure 15. (a) Power spectrum and noise figure, (b) eye diagram for concentration and length of the doped fiber ( $L = 5$  m and  $C = 3,5.10^{+24}/m^{-3}$ ).

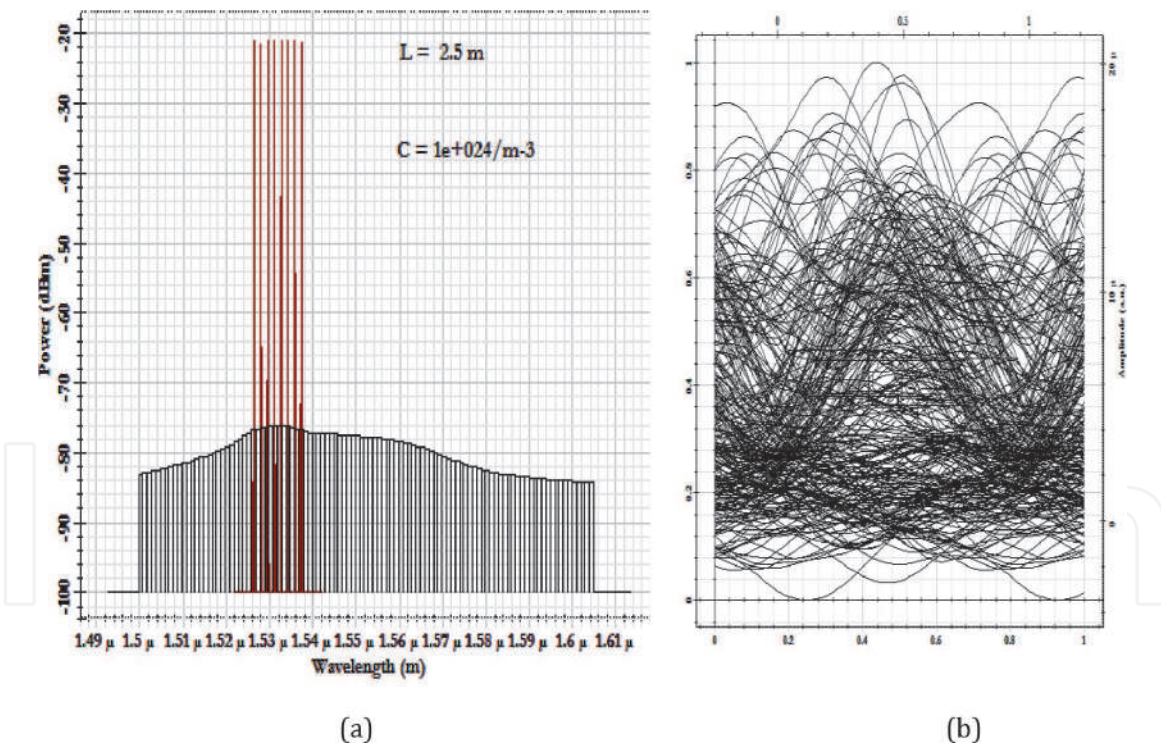


Figure 16. (a) Power spectrum and noise figure, (b) eye diagram for concentration and length of the doped fiber ( $C = 1.10^{+24}/m^{-3}$  and  $L = 2.5$  m).

Comparison of the five graphs leads to the conclusion that the gains are flattened with a  $R_G = 0.7$  in the band 1537 nm to 1545 nm wavelength around a gain of 26.3 dB with a noise Figure (NF) of less than 4 dB for 8 transmission channels for a concentration of 5,  $5.10^{24}/m^{-3}$  and a doped fiber length of 7.5 m the worst case (gain less equalized with a  $R_G = 1.54$ ) is obtained with a fiber length of 12.5 m (Table 3).

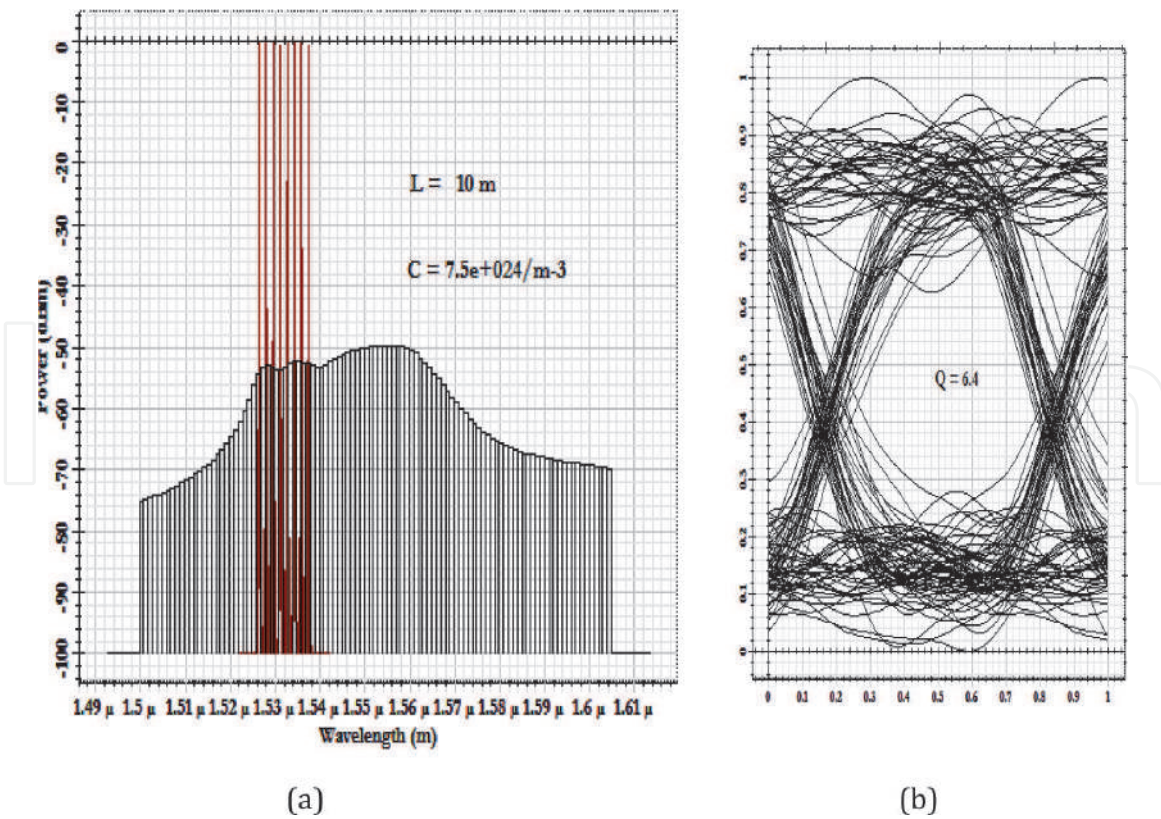


Figure 17.  
 (a) Power spectrum and noise figure, (b) eye diagram for concentration and length of the doped fiber ( $C = 7,5 \cdot 10^{+24}/m^{-3}$  and  $L = 10 \text{ m}$ ).

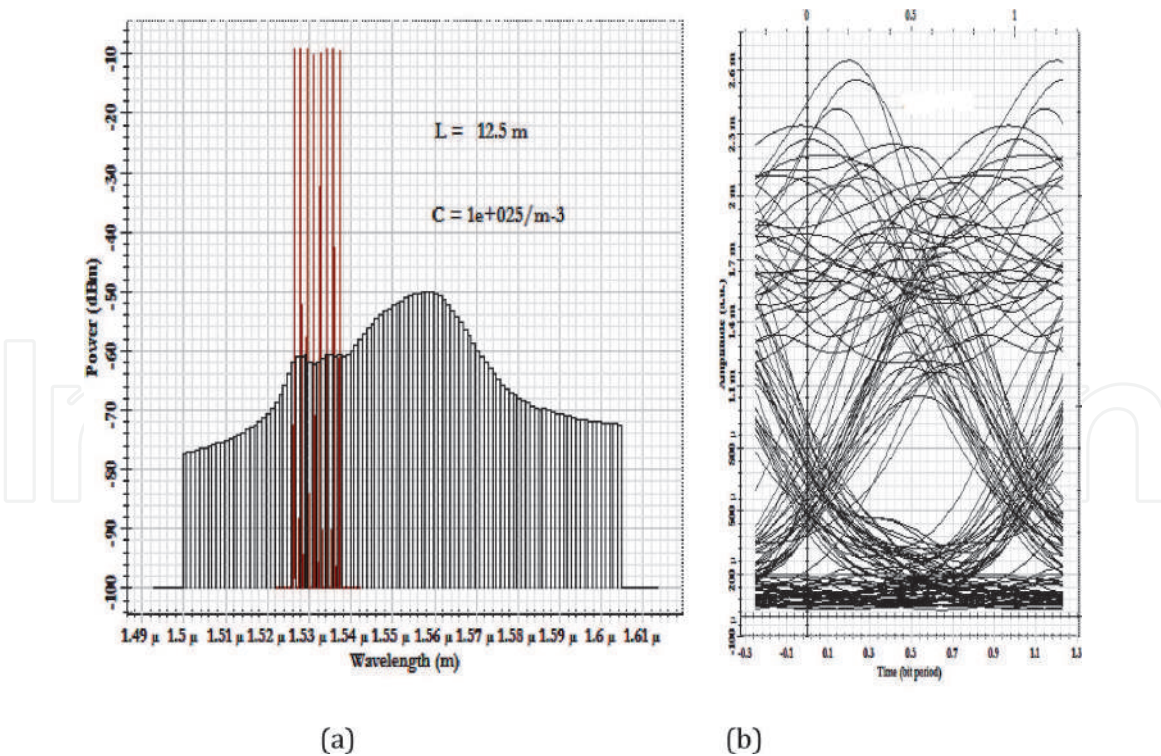


Figure 18.  
 (a) Power spectrum and noise figure, (b) eye diagram for concentration and length of the doped fiber ( $C = 1.10^{+25}/m^{-3}$  and  $L = 12,5 \text{ m}$ ).

## 6.2 Gain equalization through the use of a GFF filter

Gain Equalizing Filters, also known as GFF (Gain Flattening Filters), are integrated into optical systems and are usually combined with optical amplifiers in the

Gain	NF	$R_G = G_{max} - G_{min}$	$R_{NF} = NF_{max} - NF_{min}$	Concentration "N"	L
2.95 dB	1.95 dB	0.08 dB	0.46 dB	$1.10^{24}/m^3$	2.5 m
19.44 dB	3.43 dB	0.47 dB	1.63 dB	$3.5.10^{24}/m^3$	5 m
26.63 dB	3.65 dB	0.70 dB	2.15 dB	$5.5.10^{24}/m^3$	7.5 m
23.59 dB	4.47 dB	0.98 dB	2.04 dB	$7.5.10^{24}/m^3$	10 m
14.71 dB	4.66 dB	1.54 dB	2.06 dB	$1.10^{25}/m^3$	12.5 m

**Table 3.**  
Optimization results obtained by the WDM analyzer.

transmission chain to ensure good gain flattening. This process provides a solution to the problem of equalizing the amplifier output power of a WDM multiplexed system. This part refers to a process of combining the EDFA amplifier with a GFF filter and visualizing the power and noise spectrum.

The tables below show the results of the WDM analyzer at the output of the EDFA “Table 4” and the output of the gain equalizing filter “Table 5” in terms of wavelength, gain, noise figure and the deference between the maximum and minimum values of these figures. Comparison between the tables below leads to the conclusion that the gains are flattened with a  $R_G = 0.77$  in the band 1537 nm to 1545 nm wavelength around a gain of 26.97 dB with a noise Figure (NF) of less than 2.15 dB for 8 transmission channels.

The figures below show a schematic representation of the spectrum emitted at the output of the EDFA and output of the gain equalizing filter GFF. In Figure 19, the different wavelengths of the multiplex at the output of the EDFA (at the input of the filter) can be recognized, represented by red symbols from 1 to 8. It can be seen that the spectrum received at the output of the EDFA has a different total

Wavelength (nm)	Gain (dB)	Noise Figure (dB)
1537.4	27.859	4.017
1535.82	29.448	3.368
1534.25	31.714	3.913
1532.68	32.990	3.382
1531.12	32.764	3.144
1529.55	31.265	2.382
1527.99	29.096	2.971
1526.44	26.298	2.063
	Gain (dB)	Noise Figure (dB)
<b>Min value</b>	26.197	2.0631
<b>Max value</b>	32.994	4.026
<b>Total</b>	30.712	0
<b>Ratio Maxmin</b>	6.698	1.954
	nm	nm
<b>Wavelength at</b>	1526.44	1526.44
<b>Wavelength at</b>	1537.40	1537.40

**Table 4.**  
Results of the WDM analyzer at the EDFA output.

Wavelength (nm)	Gain (dB)	Noise Figure (dB)
1537.4	26.976	3.697
1535.82	26.687	3.991
1534.25	26.864	4.026
1532.68	26.634	3.297
1531.12	26.364	3.169
1529.55	26.464	2.928
1527.99	26.803	2.597
1526.44	26.197	1.871
	Gain (dB)	Noise Figure (dB)
<b>Min value</b>	26.197	1.871
<b>Max value</b>	26.864	4.026
<b>Total</b>	26.628	0
<b>Ratio Maxmin</b>	0.778	2.155
	nm	nm
<b>Wavelength at</b>	1526.44	1526.44
<b>Wavelength at</b>	1537.40	1537.40

**Table 5.**  
 WDM analyzer filter GFF output results.

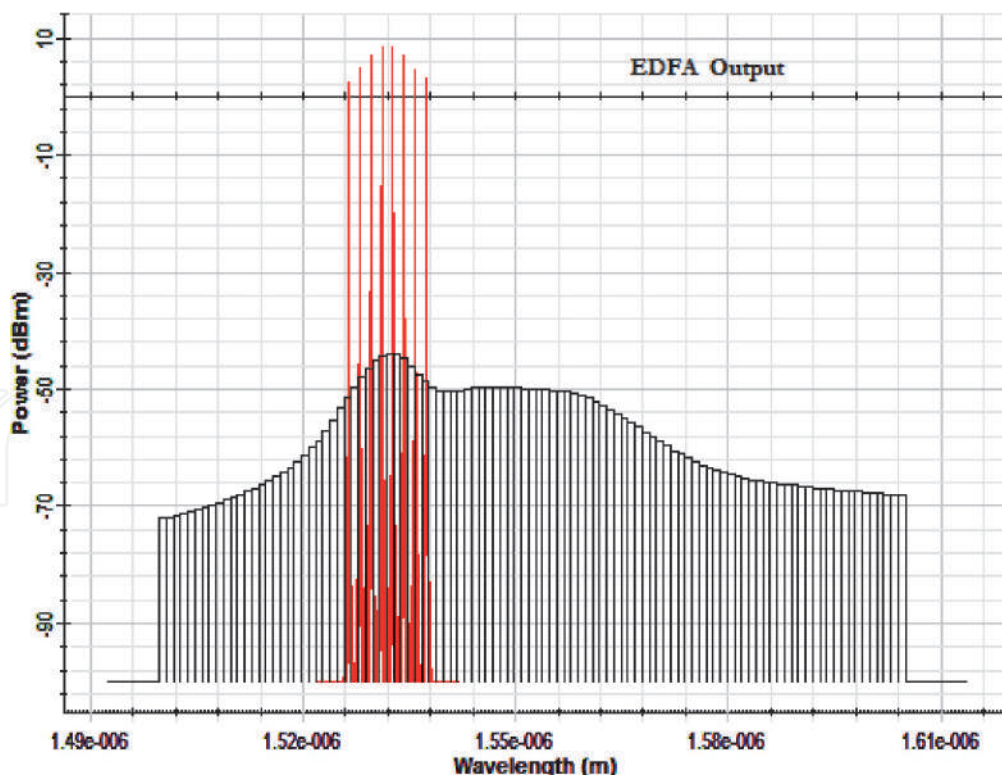


**Figure 19.**  
 Power spectrum and noise figure at EDFA output.

power for the different wavelengths while the spectrum received at the output of the filter has a total power which is substantially equal and in particular the gain is flat over the amplification band **Figure 20**.

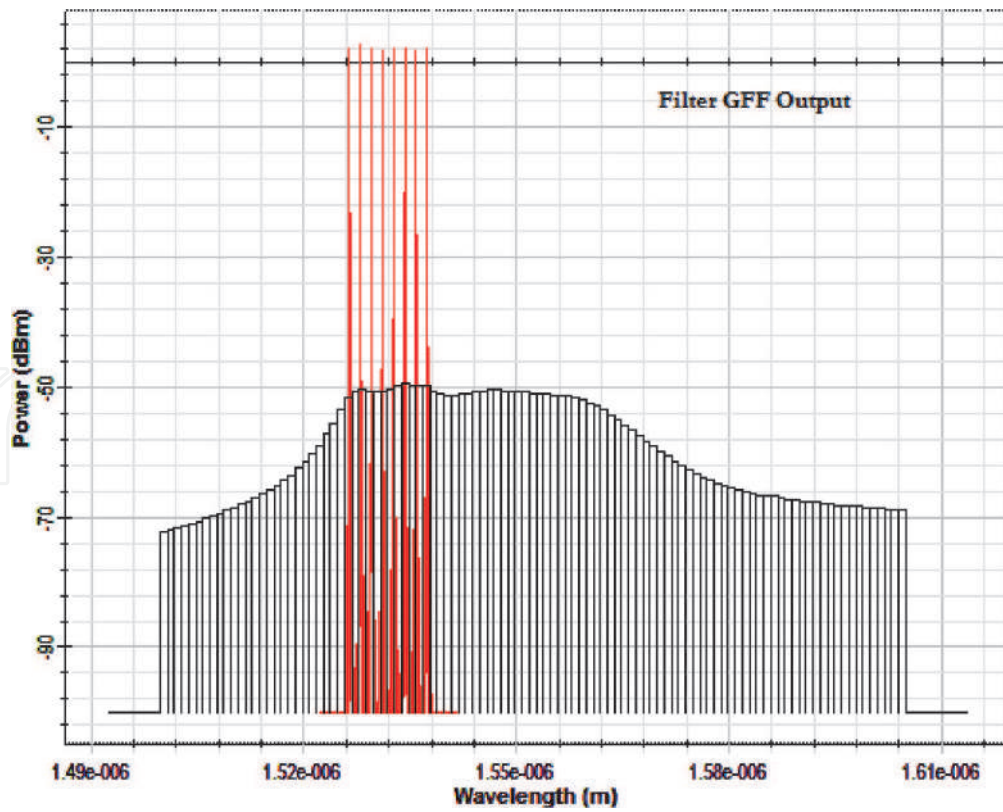


**Figure 20.**  
Power spectrum and noise figure at filter FGG output.

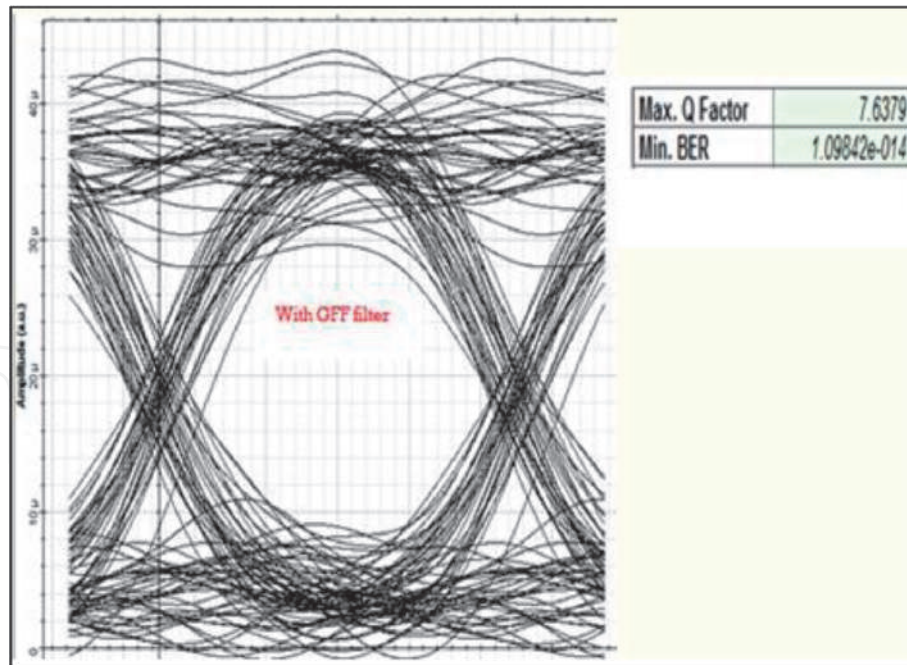


**Figure 21.**  
Eye diagram of the WDM/FSO with GFF filter.

According to the eye diagrams for both cases we can clearly see the aperture of diagram **Figure 21** compared to diagram **Figure 22**; this confirms that the use of the gain equalizing filter GFF improves the quality of the amplified WDM system.

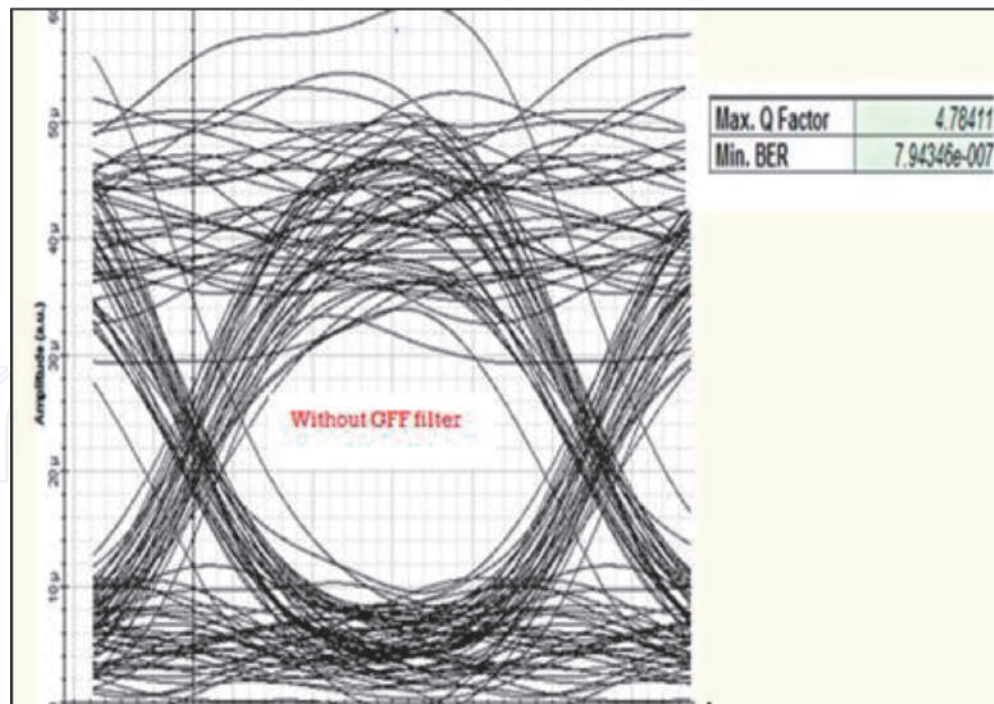


**Figure 22.**  
*Eye diagram of the WDM/FSO without GFF filter.*

## 7. Conclusion

This chapter summarizes the simulation results and their interpretations of the comparison of two configurations of EYDWA (post-and preamplifier) in the WDM/FSO system. The mentioned amplifiers were evaluated based on values of BER and the quality -factor. WDM over FSO communication system is very suitable and effective in providing high data rate transmission with low bit error rate (BER). Therefore, WDM – FSO system has achieved very good results, it has many problems, such as heavy attenuation coefficient.

For the heavy rain condition the maximum link range about 8 km at  $BER = 10^{-9}$ . Also, It can be noticed from simulation that the best results achieved EYDWA post-amplifier configuration, this later was able to reach transmission distance of WDM/FSO up to 26 Km however the worst results in terms of FSO range are obtained with EYDWA preamplifier and the distance of transmission is limited at 16 Km.

Furthermore the gain flatness and the noise figure of EDFA have been studied. The gain non-uniformity for each channel using the optimization of erbium doped and length fiber doped in order to equalize the amplitude gain in the WDM-FSO system have been simulated. The simulation results prove that the proposed method by optimization of erbium doped and length of fiber doped offers and improved the best performance in terms of the gain flatness  $GF = 0.7$  for fiber length  $L = 7.5$  m and erbium concentration  $C = 5,5.10^{+24}/m^{-3}$ .

IntechOpen

### **Author details**

Bentahar Attaouia<sup>1\*</sup>, Kandouci Malika<sup>2</sup>, Ghouali Samir<sup>3</sup> and Dinar Amina Elbatoul<sup>3</sup>

1 University of Mascara, LEPO Laboratory of sidi bel abbes, Algeria

2 University of sidi bel abbes, LEPO Laboratory of sidi bel abbes, Algeria

3 University of Mascara, Algeria

\*Address all correspondence to: bentaha\_1011@yahoo.fr

### **IntechOpen**

---

© 2022 The Author(s). Licensee IntechOpen. This chapter is distributed under the terms of the Creative Commons Attribution License (<http://creativecommons.org/licenses/by/3.0>), which permits unrestricted use, distribution, and reproduction in any medium, provided the original work is properly cited. 

## References

- [1] Makowski M, Sypek M, Kolodziejczyk A. Colorful reconstructions from a thin multi-plane phase hologram. *Optics Express*. 2008; **16**:11618 Available from <http://www.opticinfobase.org/oe/abstract.cfm?URI=oe-16-15-11618>
- [2] Dat PT et al. Performance evaluation of an advanced DWDM RoFSO system for heterogeneous wireless. In: Tavel P, editor. *Modeling and Simulation Design*. AK Peters Ltd.; 2007
- [3] Arora P, Kumar S, Sharma D. Performance analysis of NRZ and RZ modulation schemes in optical fiber link using EDFA. *International Journal of Advanced Research in Computer Science and Software Engineering (IJARCSSE)*. 2017;7(8): 2277-2128
- [4] Chaudhary S, Lin B, Tang X, et al. 40 Gbps–80 GHz PSK-MDM based Ro-FSO transmission system. *Optical and Quantum Electronics*. 2018;50:321
- [5] Attaouia B, Malika K. Performance improvement by pre-amplifying with erbium, ytterbium doped devices link extenders of fiber to the home. *International Journal of Information Engineering and Electronic Business*. 2016;8(4) MECS.:26-34 Available from <http://www.mecspress.org>
- [6] Delavaux J-MP et al. Lossless 40 Channel Waveguide Demultiplexer for 10 Gbit/s DWDM Fiber Transmission Experiment. *ECOC*; 2000 paper 10.3.6
- [7] Philipsen J et al. Compact Gain-Block Consisting of an Er<sup>+</sup>-Doped Waveguide Amplifier (EDWA) and a Pump/Signal Multiplexer, Realized by Ion Exchange. *OAA*; 2000 paper OTuD2
- [8] Enns K, Taccheo S, Rogowski T, Shmulovich J. Efficient Erbium-doped waveguide amplifier insensitive to power fluctuations. *Optics Express*. 2006;14(22):10307-10312
- [9] Di Pasquale F, Federighi M. Improved gain characteristics in high-concentration Er<sup>3+</sup>/Yb<sup>3+</sup> Codoped glass waveguide amplifiers. *IEEE Journal of Quantum Electronics*. 1994;30(9): 2127-2131
- [10] Muhammad OH, Hifsa S. Septechieving high gain using Er-Yb codoped waveguide/fiber optical parametric hybrid amplifier for dense wavelength division multiplexed system. *Optical Engineering*. 1994;57: 2127-2131 id. 056108 (2018)
- [11] Mahrana O, Moustafa H, et al. High performance characteristics of dual pumped Er<sup>3+</sup>/Yb<sup>3+</sup> co-doped/raman hybrid optical amplifier. *Journal of Optoelectronics and Advanced Materials*. 2016;18(7–8):595-601
- [12] Wang XJ, Yuan G, Isshiki H, Kimura T, Zhou Z. Photoluminescence enhancement and high gain amplification of ErxY2–xSiO5 waveguide. *J. Appl. Phys. Lett.* 2010; **108**:013506
- [13] Kaur H, Sarangal H. Simulative investigation of FSO system using 4X4 transmitter receiver combination integrated with various types of amplifiers under different weather conditions. *International Journal of Signal Processing*. 2016;9(3): 11-16
- [14] Jiang C, Zeng Q. Optimization of erbium-doped waveguide amplifier. *Optical and Laser Technology*. 2004; **36**(2):167-171
- [15] Berkedmir C, Ozsoy S. Numerical analysis of the signal gain and noise figure of Yb<sup>3+</sup>/Er<sup>3+</sup> doped fiber amplifier

at different pumping power configurations. *Optical Materials*. 2008; **31**:229-232. DOI: 10.1016/j.optmat.2008.03.016 [Citation Time(s):1]

[16] Li JF, Duan KL, Wang YS, Zhao W, Guo YK, Lin XD. Modeling and optimizing of high-concentration erbium-doped fiber amplifiers with consideration of ion-clusters. *Optics Communications*. 2007;**277**(1):143-149

IntechOpen

# We are IntechOpen, the world's leading publisher of Open Access books Built by scientists, for scientists

6,300

Open access books available

171,000

International authors and editors

190M

Downloads

Our authors are among the

154

Countries delivered to

TOP 1%

most cited scientists

12.2%

Contributors from top 500 universities



WEB OF SCIENCE™

Selection of our books indexed in the Book Citation Index  
in Web of Science™ Core Collection (BKCI)

Interested in publishing with us?  
Contact [book.department@intechopen.com](mailto:book.department@intechopen.com)

Numbers displayed above are based on latest data collected.  
For more information visit [www.intechopen.com](http://www.intechopen.com)



# Phase Noise in OFDM

*Kamayani Shrivastav*

## Abstract

Orthogonal frequency division multiplexing (OFDM) technique provides high data rate with high spectral efficiency for operating close to the Shannon capacity bounds. With the advantages of simple channel equalization, robustness against frequency selectivity of the channel, and efficient implementation, this is a widely deployed technique. Orthogonal frequency division multiplexing access (OFDMA), the multiple access technique using OFDM, has the great potential for providing high spectral efficiency due to its integrated space-frequency and multiuser diversity. Besides all the advantages, OFDM/A is very susceptible to transceiver's impairments such as phase noise (PHN), carrier frequency offset, and in-quadrature phase imbalance effect. Phase noise is the random fluctuation in phase of the sinusoidal waveform used for frequency up/down conversion of baseband signals to/from RF (radio frequency). This occurs due to the inherent imperfections of oscillators used for this purpose. This chapter addresses the orthogonal frequency division multiplexing/multiple access system performance under the impact of transceiver oscillator phase noise.

**Keywords:** multi carrier (MC), common phase error (CPE), intercarrier interference (ICI), multiuser interference (MUI), free-running oscillator (FRO), phase-locked loop (PLL)

## 1. Introduction

Orthogonal frequency division multiplexing (OFDM) is a multicarrier modulation technique to represent the information, which reduces the complexity of receiver digital processing unit while combating the deleterious effects of the channel with simple correction algorithms. It enables one-tap equalization by cyclic prefix (CP) insertion even in frequency selective channel and the use of discrete Fourier transform (DFT) and its extremely efficient and well-established fast Fourier transform (FFT) algorithm for implementation has made it amenable in terms of cost also [1–3]. However, some of the immediate consequences of these compelling benefits in OFDM are: limiting the spectral efficiency because of CP insertion, deleterious impact of high peak-to-average power ratio (PAPR), and serious sensitivity toward transceivers' impairments [4, 5]. The transceivers' impairments, such as phase noise (PHN), carrier frequency offset (CFO), and in-quadrature phase (IQ) imbalance effect, need to be addressed significantly to make the best possible use of limited radio spectrum to further increase throughput as well as user capacity.

While there are many transceivers' impairments that are to be taken into consideration in designing a digital communication system, there is a convincing reason to focus on the PHN precisely. While CFO and IQ imbalance is deterministic, PHN on the other hand is random perturbations in the phase of the carrier signal

generated by the transceiver oscillators [6–10]. Moreover, the multicarrier systems, such as OFDM, suffer a much loss in signal-to-noise ratio (SNR) due to PHN than single carrier systems. This is the result of longer duration of multicarrier symbol and the loss of orthogonality between the subcarriers. Further, PHN severely limits the performance of systems that employ dense constellations and degradation gets more pronounced in high-carrier-frequency systems.

## 2. Phase noise

The autonomous system, oscillator provides a periodic sinusoidal reference signal used for up/down conversion of the baseband/RF signal to/from RF/baseband frequency. In practice, wireless digital communication systems use either oscillator in isolation, known as free-running oscillator (FRO) or phase-locked loop (PLL) oscillator because of its high stability and easy control. Either FRO or PLL voltage control oscillator (VCO), in an ideal oscillator for a perfect periodic signal: the transition of phase over a time interval should be constant, whereas practically this phase increment is a random variable. This random variation of phase is phase jitter and its instantaneous deviation is called PHN [11–13]. Thus, the output of a practical oscillator is noisy and can be written as:

$$s(t) = [A + a(t)] \sin [\omega_c t + \theta(t)] \quad (1)$$

where  $A$  and  $\omega_c = 2\pi f_c$  are amplitude and angular frequency, respectively, and  $a(t)$  is amplitude fluctuation, which can be kept in limit by using an automatic gain control (AGC).  $\theta(t)$ , the phase fluctuation (time-varying PHN), is very difficult to mitigate and can have major impact on system performance.

Phase fluctuations, resulting in the random shifting of oscillator frequency, have its origin in the noise sources present in the internal circuitry of an oscillator. These noise sources can be categorized into white (uncorrelated) and color (correlated) noise sources [14]. The white noise has the flat power spectral density (PSD) where the PSD of color noise is proportional to  $1/f$ . The generated PHN in an oscillator, because of these white and color noise sources, has two components. First is resulting from direct amplification/attenuation of the white and color noise, and the second is due to the phase change of white and color noise, which happens because of the time integration of white and color noise [11–14].

Resulting oscillator PHN spectrum is shown in **Figure 1** where PSD is plotted against frequency  $f$ . White PHN (flat) and white frequency-modulated (FM) PHN ( $1/f^2$ ) spectra are resulting with white noise sources and flicker PHN ( $1/f$ ) and flicker FM PHN ( $1/f^3$ ) spectra are resulting with color noise sources.

For FRO:

$$\theta_{n+1} = \theta_n + \phi_n \quad (2)$$

which is Wiener process [15] with mean zero and variance,  $\sigma_{\phi_n}^2 = \sigma_{\phi}^2 = 2\pi\beta T_s/N$  where  $\beta = 2\Delta f_{3dB}$ , double of 3 dB bandwidth.

For PLL VCO [16].

$$\theta_{n+1} = \theta_n e^{-\frac{T_s}{N}} + \phi_{PLLn} \quad (3)$$

which is celebrated O-U process where  $\phi_{PLLn}$  is a sequence of identically and independently distributed (iid) random variables with mean zero and variance:

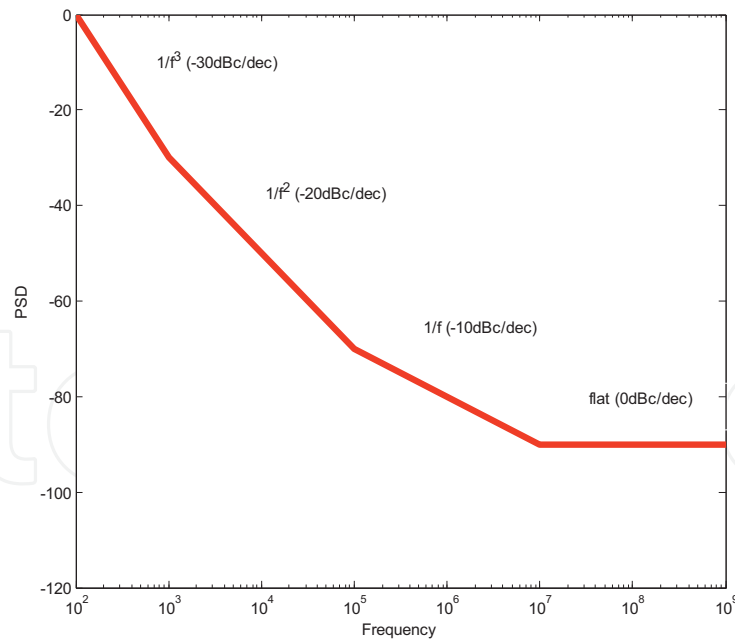


**Figure 1.**  
 PSD of PHN in oscillator output.

$$\sigma_{\phi_{PLL_n}}^2 = 4\pi^2 f_c^2 \left( C_{RO} \frac{T_s}{N} + 2 \sum_{i=1}^2 (\xi_i + \zeta_i) \left( 1 - e^{-\lambda_i \frac{T_s}{N}} \right) \right).$$

where:

$$\lambda_{1,2} = \frac{\omega_{lpf} \pm \sqrt{(\omega_{lpf}^2 - 4\omega_{lpf} \sqrt{C_{PLL}})}}{2},$$

$$\xi_1 = \frac{C_{RO}\lambda_2}{(\lambda_1 - \lambda_2)\lambda_1}, \xi_2 = \frac{-C_{RO}\lambda_1}{(\lambda_1 - \lambda_2)\lambda_2},$$

$$\zeta_1 = \frac{C_{RO} + C_{VCO}}{(\lambda_1 - \lambda_2)^2} \left( \frac{\lambda_2^2}{2\lambda_1} - \frac{\lambda_1\lambda_2}{2(\lambda_1 + \lambda_2)} \right),$$

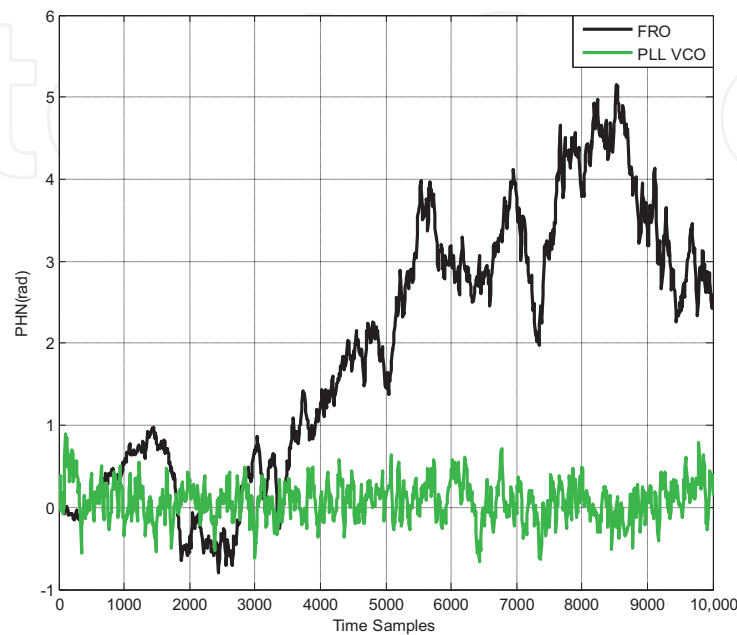


**Figure 2.**  
 PHN time samples for FRO and PLL VCO.

$f_c$	5 GHz
$\beta$	20 kHz
$f_{lpf}$	20 kHz
$C_{RO}$	$10^{-25}$ s
$C_{VCO}$	$10^{-19}$ s
$C_{PLL}$	$4 * 10^8 / s^2$

**Table 1.**  
PHN modeling parameters.

and

$$\zeta_2 = \frac{C_{RO} + C_{VCO}}{(\lambda_1 - \lambda_2)^2} \left( \frac{\lambda_1^2}{2\lambda_2} - \frac{\lambda_1\lambda_2}{2(\lambda_1 + \lambda_2)} \right)$$

where  $f_c$  is the center frequency of VCO in Hz,  $\omega_{lpf}$  is the angular corner frequency of the low-pass filter in rad/sec, and  $\sqrt{C_{PLL}}$  is the PLL bandwidth in Hz.  $C_{RO}$  and  $C_{VCO}$  are diffusion rates of the reference oscillator (RO) and VCO, respectively.

The simulated samples of PHN modeled as Wiener process and celebrated O-U process, for FRO and PLL VCO, respectively, are shown in **Figure 2**. Though the time-varying PHN process of FRO can be characterized with  $\beta$  only, PLL VCO requires more parameter to characterize such as given in **Table 1**, assuming that the VCO is noisier than reference oscillator.

### 3. OFDM

OFDM is a low complex modulation/multiplexing multicarrier (MC) technique to modulate  $N$  orthogonal sub carriers with  $N$  complex-valued source symbols  $X_k, k = 0, 1, \dots, N - 1$ , efficiently by using digital signal processing. The source symbol is achieved after source coding, interleaving, and channel coding if applicable. The source symbol duration  $T_d$  of the serial data symbol results in the OFDM symbol duration:  $T_s = N T_d$ .

From the **Figure 3**, the frequency domain received signal on the  $k^{th}$  subcarrier of the  $m^{th}$  symbol is without ISI and ICI and is given by:

$$y_k^m = X_k^m h_k + W_k^m \quad 0 \leq k \leq N - 1 \quad (4)$$

where  $X_k^m$  is  $k^{th}$  element of symbol vector  $X^m$ ,  $h_k$  is the  $k^{th}$  element of channel vector  $\mathbf{h} = [h_0, h_1, h_2, \dots, h_{N-1}]^T$ ,  $W_k^m$  is AWGN in frequency domain. It is preferable to represent the signal model in matrix form as:

$$\mathbf{Y}^m = \mathbf{D}^m \mathbf{F} \mathbf{g} + \mathbf{W}^m \quad (5)$$

where  $\mathbf{Y}^m = [y_0^m, y_1^m, \dots, y_{N-1}^m]^T$ ,  $\mathbf{F}$  is the  $N \times L$  DFT matrix with  $F(n, l) = \exp\left(-\frac{j2\pi nl}{N}\right)$ ,  $\mathbf{D}^m = \text{diag}[X_0^m, X_1^m, \dots, X_{N-1}^m]$  and  $\mathbf{g} = [g(0), g(1), \dots, g(L-1)]^T$  is the time domain channel vector.  $\mathbf{W}^m = [W_0^m, W_1^m, \dots, W_{N-1}^m]^T$ , is an uncorrelated

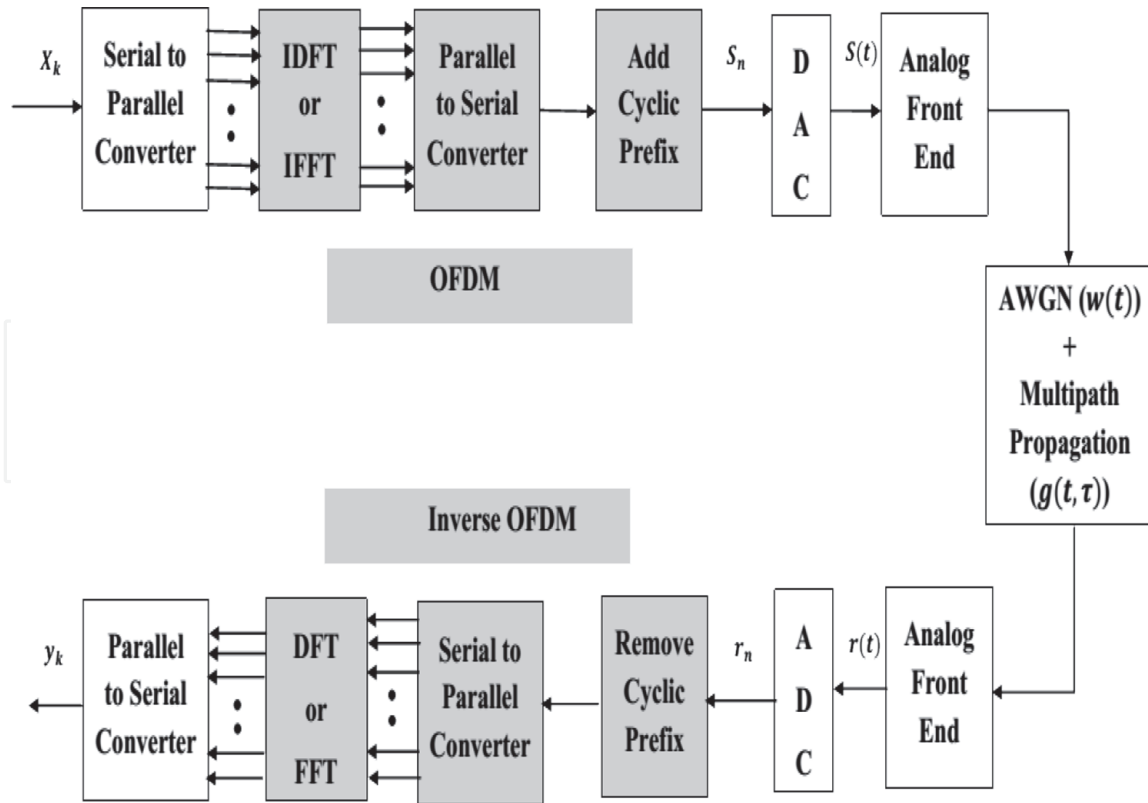


**Figure 3.**  
 OFDM modulation and demodulation.

white noise vector distributed as,  $\Pr(\mathbf{W}^m) = \mathcal{CN}(0, 2\sigma_\omega^2 \mathbf{I})$  with mean zero and covariance matrix  $2\sigma_\omega^2 \mathbf{I}$ , which says:

$$\Pr(\mathbf{W}^m) = \frac{1}{(2\pi)^N \sigma_\omega^{2N}} \exp\left(\frac{-1}{2\sigma_\omega^2} \mathbf{W}^{mH} \mathbf{W}^m\right). \quad (6)$$

#### 4. Phase noise in OFDM

Further to model an OFDM system with receiver PHN consisting of  $N$  subcarriers with sampling instant  $T_s/N$ , we denote the discrete-time receiver PHN impairment to the  $n^{\text{th}}$  subcarrier of the  $m^{\text{th}}$  symbol by  $\theta_n^m$  than the received OFDM signal after down conversion and CP removal can be written as [17–19]:

$$r_n^m = [S_n^m \otimes g(n)] e^{j\theta_n^m} + w_n^m, 0 \leq n \leq N - 1. \quad (7)$$

If  $\theta^m = [\theta_0^m, \theta_1^m, \dots, \theta_{N-1}^m]^T$ , is the PHN vector for the  $m^{\text{th}}$  OFDM symbol, then:

$$\mathbf{P}^m = \left[ p_{-\frac{N}{2}}^m, p_{-\frac{N}{2}+1}^m, \dots, p_0^m, \dots, p_{\frac{N}{2}-2}^m, p_{\frac{N}{2}-1}^m \right]^T \quad (8)$$

defines a vector of the DFT coefficients of one realization of  $e^{j\theta_n}$  during  $m^{\text{th}}$  OFDM symbol where:

$$p_k^m = \frac{1}{N} \sum_{n=0}^{N-1} e^{j\theta_n^m} e^{-j2\pi nk/N}, -\frac{N}{2} \leq k \leq \frac{N}{2} - 1 \quad (9)$$

After taking the FFT of  $r_n^m$ , the frequency domain received signal on the  $k^{\text{th}}$  subcarrier of the  $m^{\text{th}}$  symbol is:

$$y_k^m = \sum_{q=0}^{N-1} X_q^m h_q p_{(k-q)}^m + W_k^m, 0 \leq k \leq N-1 \quad (10)$$

where  $X_q^m$  is  $q^{\text{th}}$  element of symbol vector  $\mathbf{X}^m$ ,  $h_q$  is the  $q^{\text{th}}$  element of channel vector  $\mathbf{h} = [h_0, h_1, h_2, \dots, h_{N-1}]^T$ ,  $W_k^m$  is AWGN in frequency domain, and  $p_{(k-q)}^m$  is the  $(k-q)^{\text{th}}$  spectral component of PHN spectral component vector,  $\mathbf{P}^m$ , with modulo  $N$  indexing. Further note that with modulo  $N$  indexing, the lower-order spectral components of PHN are given by  $p_0, p_1, p_{N-1}, p_2, p_{N-2}$ , etc. For convenience of the later analysis, it is preferable to represent the signal model in matrix form as:

$$\mathbf{Y}^m = \mathbf{H}^m \mathbf{P}^m + \mathbf{W}^m \quad (11)$$

where

$\mathbf{Y}^m = [y_0^m, y_1^m, \dots, y_{N-1}^m]^T$ ,  $\mathbf{P}^m = [p_0^m, p_1^m, \dots, p_{N-1}^m]^T$ ,  $\mathbf{h} = [h_0, h_1, h_2, \dots, h_{N-1}]^T$ ,  $\mathbf{X}^m = [X_0^m, X_1^m, \dots, X_{N-1}^m]^T$  and  $\mathbf{H}^m$  is a column-wise circulant matrix whose first column is vector  $[h_0 X_0^m, h_1 X_1^m, \dots, h_{N-1} X_{N-1}^m]^T$ .  $\mathbf{W}^m = [W_0^m, W_1^m, \dots, W_{N-1}^m]^T$ , is an uncorrelated white noise vector distributed as  $\Pr(\mathbf{W}^m) = \mathcal{CN}(0, 2\sigma_\omega^2 \mathbf{I})$  as given in Eq. (6).

#### 4.1 Common phase error

In single carrier (SC) systems, the phase noise merely causes simple random rotation in the symbol constellation known as common phase error (CPE). **Figure 4a** shows the received signal constellation of an SC, 16-QAM modulation over an AWGN channel (SNR = 30 dB), whereas the effect of PHN from an FRO (PHN variance = .06 rad<sup>2</sup>), on received signal constellation, is shown in **Figure 4b**.

#### 4.2 Intercarrier interference

In OFDM systems, in addition to the rotational effect, PHN also causes ICI. The ICI is present because PHN causes energy of individual subcarriers to spread on the top of all the other subcarriers [20–23]. **Figure 5** shows two systems with the bandwidth of 22 MHz where first system employs the ideal oscillator without PHN with carrier frequency 2420.5 MHz, whereas second system uses a noisy FRO with carrier frequency 2433.5 MHz, which causes spectral regrowth and results in power leakage to the first band, producing the intercarrier interference (ICI).

**Figure 6a** shows the received signal constellation of an OFDM system with 64 subcarriers, which are 16-QAM modulated over AWGN (SNR = 35 dB) with receiver PHN (both CPE and ICI) from an FRO (PHN variance = .06 rad<sup>2</sup>), whereas the effect of receiver as well as transmitter PHN from an FRO (PHN variance = .06 rad<sup>2</sup>) on received signal constellation is shown in **Figure 6b**. The constellation rotation is produced because of the CPE, whereas the cloudy constellation is impact of ICI.

The effect of PHN on BER of the OFDM system is shown in **Figure 7** for receiver FRO PHN (PHN variance = .06 rad<sup>2</sup>) only and for transceiver FRO PHN (PHN variance = .06 rad<sup>2</sup>) and is compared against the BER of pure AWGN channel.

OFDM symbols are generated using 16-quadrature amplitude modulation (QAM) and 64-point IFFT and then prepended by CP of length 16 samples before

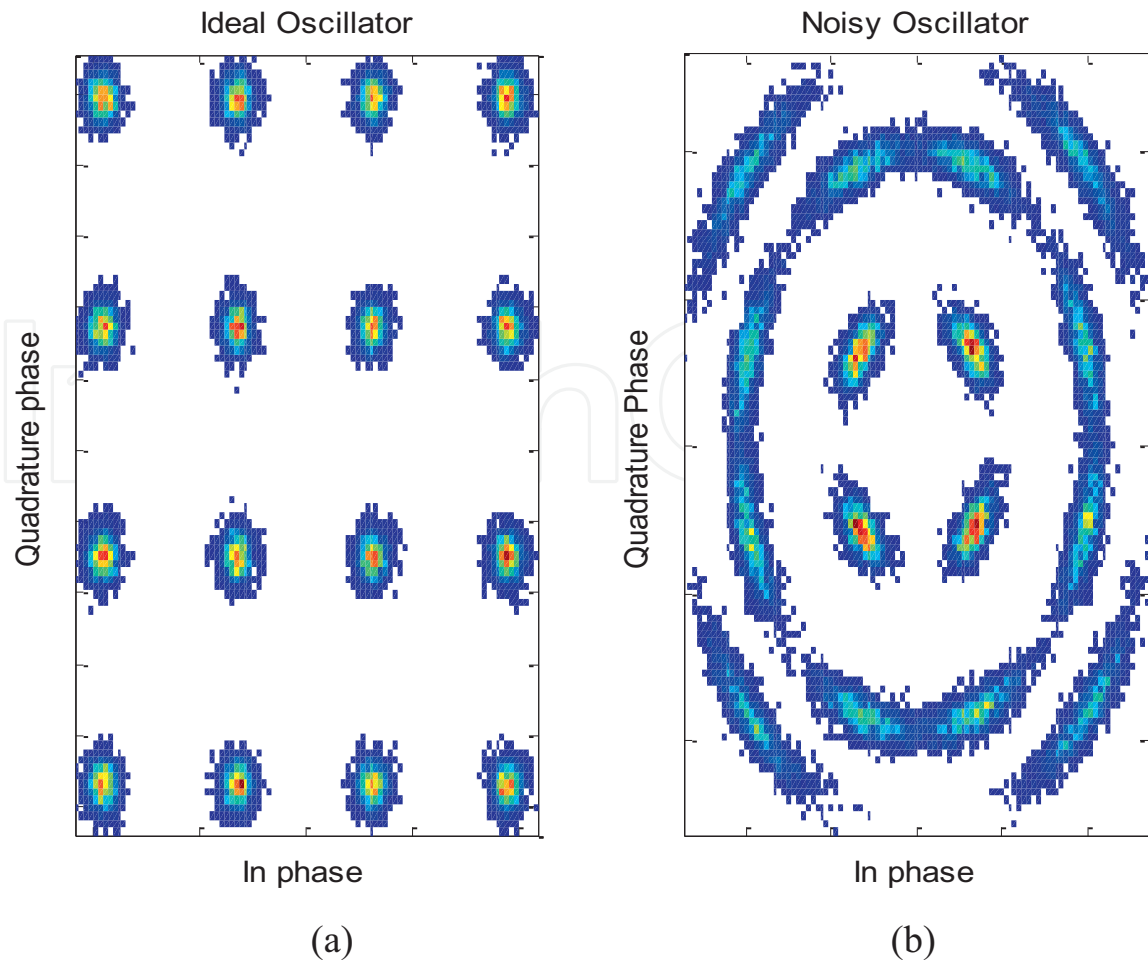


**Figure 4.**  
 Effect of phase noise in SC communication system (random rotation in constellation).

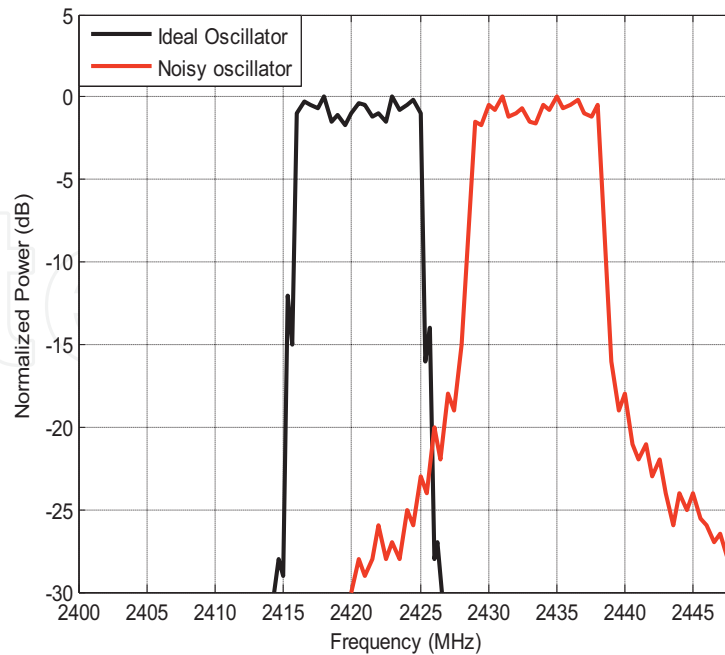
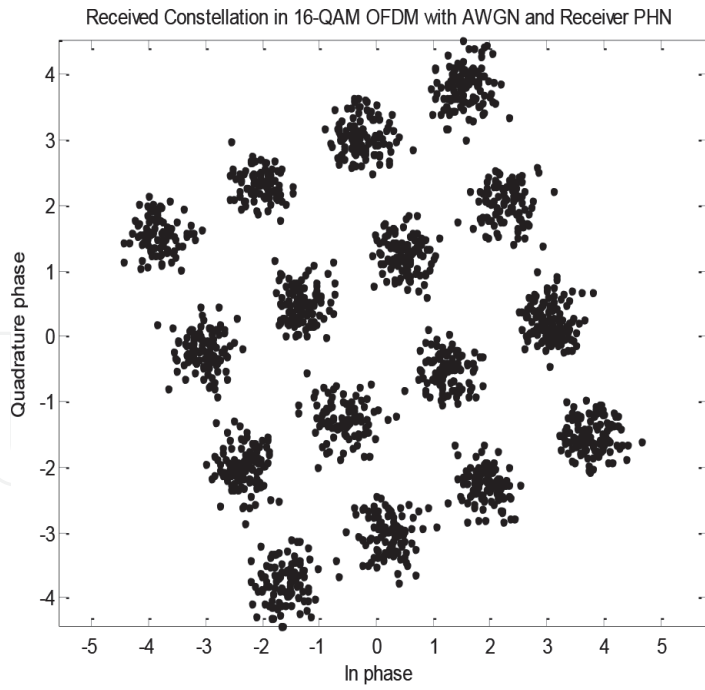
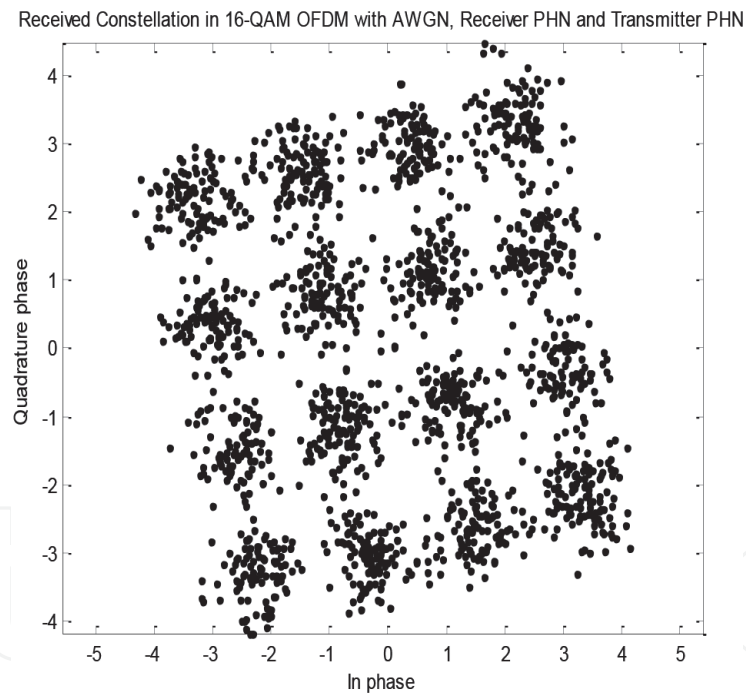


**Figure 5.**  
 Effect of phase noise in MC communication system (spectral regrowth (in-band-ICI)(out-of-band-MUI)).

transmitting over the channel. The 64-point FFT of the received signal is taken after CP removal. Simulation model is based on IEEE 802.11 g like system with parameters given in **Table 2**.



(a)



(b)

**Figure 6.** Received constellations in 16-QAM OFDM system with (a) receiver phase noise and (b) transceiver phase noise.

## 5. OFDMA

In OFDMA system, both the time and frequency resources are used to separate the multiple users. As OFDMA is typically used with burst transmission, a burst consists of many OFDM symbols. In an OFDM symbol, there are many subcarriers. So, a subcarrier in frequency domain and symbol duration in time domain are the finest units. The combination of a time unit and a frequency unit, i.e., a symbol period and a

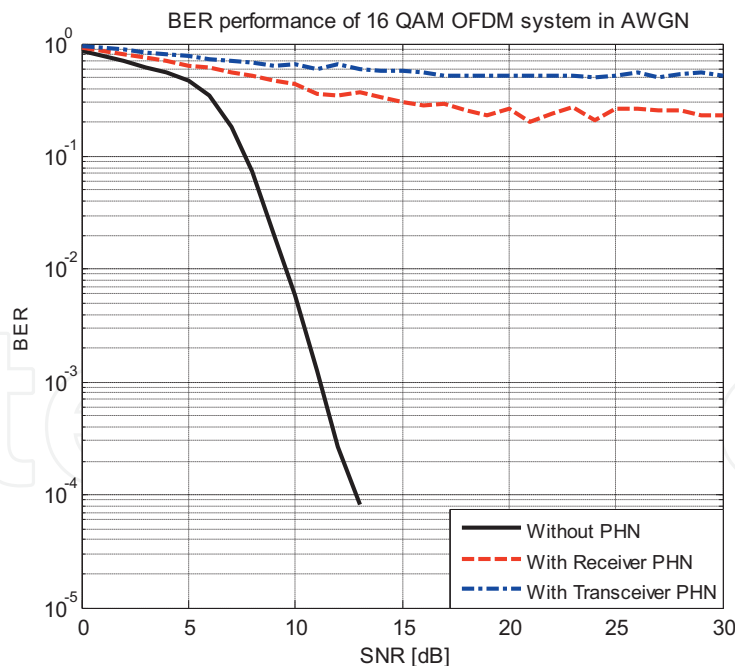


**Figure 7.**  
 16-QAM OFDM BER performance in AWGN channel with phase noise.

$F_s$	20 MHz
$N$	64
FFT Size	64
$N_g$	16 Samples
Mapping	16-QAM

**Table 2.**  
 OFDM modeling parameters.

subcarrier, is the finest slot, which or group of which is allocated to one of the multiple users. **Figure 8** shows the time frequency and power grid of OFDMA [24, 25].

Practically, in frequency domain, the allocation is not done at the level of subcarriers but on the group of subcarriers. This subcarrier's allocation is known as subchannelization. To explain the basic principle of OFDMA transceiver, we are considering here that one user is using one subcarrier in the given time slot, i.e., number of users ( $U$ ) =  $N$ . With this the simplest OFDMA uplink scheme is illustrated in **Figure 9**. At the transmitter side (mobile terminal), each user is having individual transmitters. At the receiver side (base station), the received signal is the sum of  $U$  users' signal, which acts as an OFDM signal. Because of this in OFDMA receiver, a single MC demodulator (OFDM demodulator) is required than  $U$  demodulators as in case of conventional frequency division multiple access (FDMA) system. At the transmitter side, a single transmitter consists of symbol generator and OFDMA modulator. The symbol is generated with applicable channel coding and mapping. These symbols are then OFDMA modulated with subchannelization and SC modulator (in case of  $U = N$ ) or OFDM modulator in case a single user is using group of the subcarriers.

An exact clock and carrier synchronization is must for an OFDMA system to ensure orthogonality between the unmodulated signals from different mobile terminals. This is achieved by transmitting synchronization signals from the receiver to all mobile terminals instantly. Each terminal OFDM modulator drives the carrier frequency and clock signal from these downlink signals. In case of coherent detection,

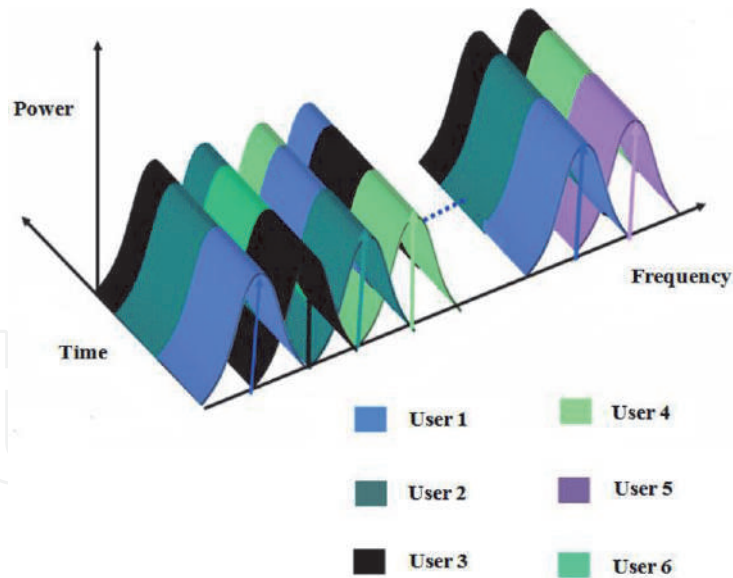


**Figure 8.**  
OFDMA time-frequency power grids [24].

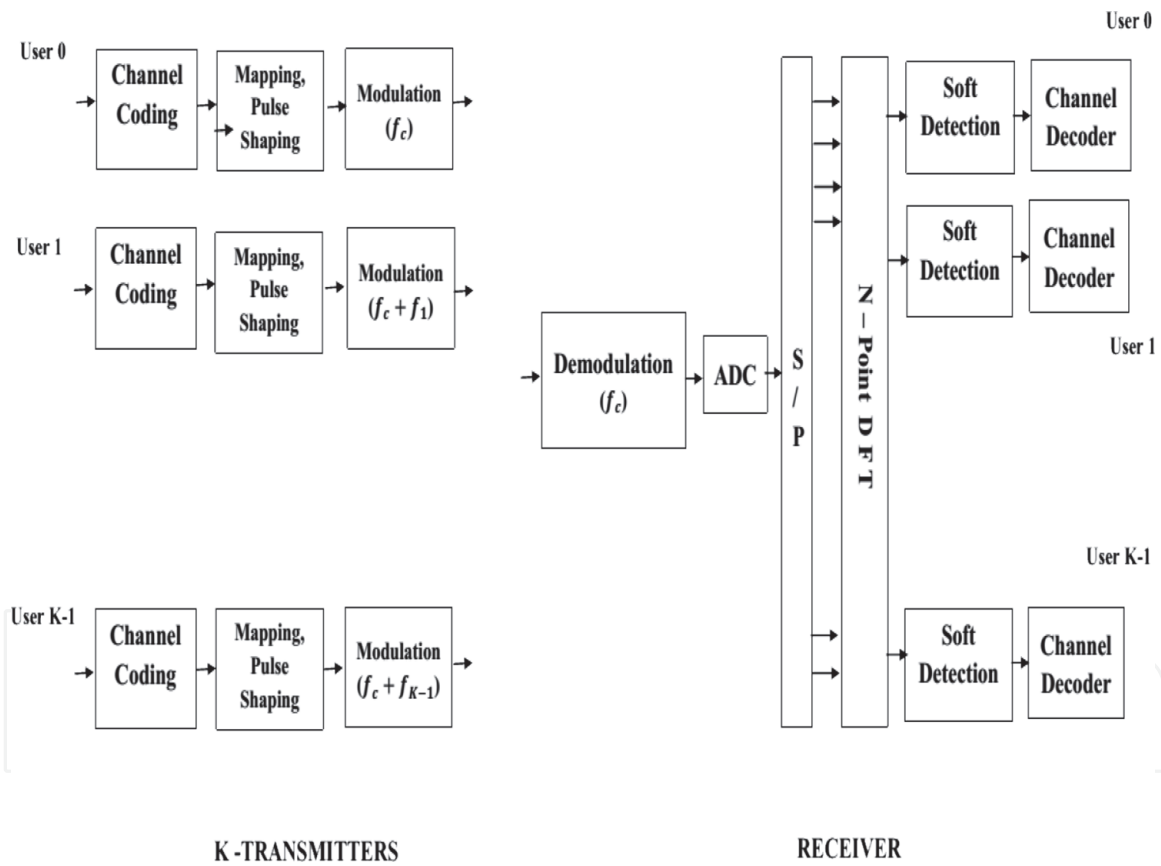


**Figure 9.**  
OFDMA uplink.

simple carrier and clock recovery circuits are sufficient in the demodulator to extract this information from the received signal as the clock and carrier frequencies are available at the base station. This factor simplifies the OFDMA demodulator.

## 6. Phase noise in OFDMA

Like all other challenges of OFDM, i.e., time and frequency synchronization, high PAPR, CFO, and IQ imbalance, OFDMA also faces the challenge of transceiver

RF impairment because of time-varying PHN. In OFDMA, CPE and in-band ICI are not the only source of interference that should be considered. The multiplexing of several users in an OFDMA scenario introduces out-of-band interference from one user on another in the OFDMA symbol. This MUI is induced by the spectral spread of the energy of each user's subcarriers on the top of other users' subcarriers. The spread is more severe in case of uplink, when there are unequal power levels as well as unequal transmitter 2(PHN 3-dB BW) for different users due to different path loss effects and different oscillator nonidealities, respectively, in an uplink scenario. Additionally, in the case of transmitter PHN, ICI results not only from the higher order components of PHN but also because of the loss of the cyclic nature and so the orthogonality is destroyed of the transmitted signal as the transmitter PHN affects the samples of the CP differently than the corresponding samples in the actual OFDMA signal part [26]. Further, the transmitter PHN impairing the CP also tends to produce ICI and hence not only  $N - 1$  but  $N + N_g - 1$  samples of PHN realization should be considered for PHN mitigation.

In regard of PHN impaired OFDMA modeling, we consider the uplink of an OFDMA with  $U(u = 1, 2, 3, \dots, U)$  users, and  $\mathcal{U}$  represents the index set of use full subcarriers with size  $\mathcal{Q}$ , means that among  $N$  subcarriers, the  $u^{th}$  user is assigned to a subset of  $\mathcal{Q}_u$  subcarriers with index set:  $\mathcal{U}_u = \{\mathcal{U}_1^u \mathcal{U}_2^u \mathcal{U}_3^u \dots \mathcal{U}_{\mathcal{Q}_u}^u\}$ , either contiguous or interleaved where  $(\cdot)^u$  denotes the  $u^{th}$  user. If  $x^{m,u}$  is the  $m^{th}$  frequency domain symbols sent by the  $u^{th}$  user, then  $k^{th}$  entry of it, say  $X_k^{m,u}$  is nonzero if  $k \in \mathcal{U}_u$ . Thereupon discrete-time baseband signal of the  $u^{th}$  user using IFFT can be represented as:

$$S_{k,n}^{m,u} = \frac{1}{N} \sum_{k \in \mathcal{U}_u} X_k^{m,u} e^{j2\pi \frac{kn}{N}}, 0 \leq n \leq N - 1. \quad (12)$$

As there is no ISI in between the windows of  $N$  samples, and that the whole processing can be done in a symbol-to-symbol manner, we drop the OFDMA symbol index  $m$  hereafter. After this the signal is transformed back to the serial form and is upconverted to RF with noisy transmitter oscillator and finally is sent over the channel. Let the discrete-time composite channel impulse response with order  $L^u$  between the  $u^{th}$  user and the uplink receiver be denoted by  $g^u(l)$  and the channel frequency response on the  $k^{th}$  subcarrier of  $u^{th}$  user's channel be denoted by  $h_k^u$ , then we have:

$$h_k^u = \sum_{l=0}^{L_k^u-1} g^u(l) e^{-j2\pi \frac{kl}{N}} \quad (13)$$

Denoting the discrete-time transmitter PHN process, receiver PHN process, and AWGN impairing to the  $u^{th}$  user by  $\theta_{T,n}^u$ ,  $\theta_{R,n}^u$ , and  $w_n$ , respectively, the received OFDMA symbol after downconversion and CP removal can be written as:

$$r_n = \sum_{u=1}^U [(S_{k,n}^u e^{j\theta_{T,n}^u}) \otimes g^u(l)] e^{j\theta_{R,n}^u} + w_n. \quad (14)$$

After taking the FFT, the frequency domain received symbol on the  $k^{th}$  subcarrier is:

$$y_k = p_0^u h_k^u X_k^u + \sum_{i=1}^U \sum_{\substack{q \in \mathcal{U}_i \\ q \neq k}} p_{k-q}^i h_q^i X_q^i + W_k. \quad (15)$$

As  $h$  is a circulant matrix, we can effectively map the transmitter PHN as receiver PHN, and by writing  $\theta_{T,n}^u + \theta_{R,n}^u = \theta_n^u$ , we have  $p_q^u = \frac{1}{N} \sum_{n=0}^{N-1} e^{j\theta_n^u} e^{-j\frac{2\pi nq}{N}}$ , and  $W_k$  is the AWGN noise in frequency domain.

From Eq. (15), we find the effect of phase noise in OFDMA to be different from that of single-user OFDM. First of all the CPE term ( $p_0^u$ ) varies according to the index  $u$ , means that each user suffers from different CPE, and they need to be considered separately for each user to estimate and mitigate.

Secondly, the summative term, called ICI, includes the user's "in-band" ICI (self-interference (SI)) and ICI caused by MUI. While including the frequency domain dummy symbols transmitted by each active user in Eq. (15), a unified frequency domain signal model can be given by:

$$y_k = \sum_{u=1}^U \sum_{q=0}^{N-1} p_{k-q}^u h_q^u X_q^u + W_k. \quad (16)$$

Splitting the summative (ICI) term is important for our analysis purpose, as MUI takes in to account the significance of the power level of users as well as the transmitter 2(PHN 3-dB BW) as these two will be significantly different for different users precisely in case of OFDMA uplink. So the signal for  $u^{th}$  user, on his  $k^{th}$  subcarrier, is given as:

$$y_k = p_0^u h_k^u X_k^u + \sum_{\substack{q \in \mathcal{U}_u \\ q \neq k}} p_{k-q}^u h_q^u X_q^u + \sum_{\substack{i=1 \\ i \neq u}}^U \sum_{\substack{q \in \mathcal{U}_i \\ q \neq k}} p_{k-q}^i h_q^i X_q^i + W_k. \quad (17)$$

First to characterize the phase noise strength in OFDMA transmission, we adopt a parameter widely used in literature, which is the relative PHN bandwidth,  $\Delta_{PN} = \frac{2(\text{PHN } 3\text{dB-BW})}{\Delta f(\text{subcarrier spacing})}$ . Having the desired advantages of OFDM transmission over single-carrier transmission with "slow" PHN model restricts to have low of this ratio, which makes the assumption of complex Gaussian distribution of the ICI false, even with higher number of subcarriers. Secondly a higher 2(PHN 3dB – BW) of the PHN process and the higher value of power level can also lead to more energy in the MUI factor of ICI terms. Considering these two facts and the OFDMA uplink scenario, not all the  $U - 1$  users will produce the MUI for  $u^{th}$  user but only those who will satisfy the following inequality will be the disruptive users for  $u^{th}$  (user)

$$\sum_{a=1}^{N-1} E \left[ |p_a^u|^2 \right] < \sum_{a=1}^{N-1} E \left[ |p_a^j|^2 \right] \text{ for } j = 1 \text{ to } U \text{ and } j \neq u. \quad (18)$$

Here we define a subset of users for the  $u^{th}$  user  $I_u, \forall j \in I_u$  with size  $I_u$ . Since the PSD of phase noise tapers off rapidly beyond the loop bandwidth, most of the energy in a phase noise sequence is contained in the frequency components corresponding to the first few orders. Hence, the largest contribution to interference on a particular subcarrier is likely to come from users occupying adjacent subcarriers. As a result, disruptive users who are occupying subcarriers adjacent to the  $u^{th}$  user are likely to be most disruptive users. Keeping this valid, Eq. (17) can be rewritten while using Eq. (18) as:

$$y_k = p_0^u h_k^u X_k^u + \sum_{\substack{q \in \mathcal{U}_u \\ q \neq k}} p_{k-q}^u h_q^u X_q^u + \sum_{i \in \mathcal{I}_u} \sum_{\substack{q \in \mathcal{U}_i \\ q \neq k}} p_{k-q}^i h_q^i X_q^i + W_k \quad (19)$$

where the second term is SI, and third term is MUI.

## 7. Conclusion

Analyzing the impact of transceiver PHN necessitates the accurate mathematical modeling of generated PHN. As the FRO model is easy to simulate mathematically and PLL is widely used in practice for digital communication systems, the PHN modeling for both of the oscillators is presented. With the white noise sources in the oscillator circuitry, the PHN is modeled as Wiener process and celebrated O-U process, for FRO and PLL VCO, respectively.

OFDM, as a low complex modulation technique, became the potential contender for MC transmission to combat the frequency selectivity of the channel. The synchronization unit (including the time and frequency synchronization units) of OFDM demodulator is performing the robust digital synchronization and channel estimation with digital algorithms. The presence of transceiver PHN degrades the OFDM system performance because of the rotational effect CPE and spectral regrowth ICI.

Being effective in mitigating the hostile channel selectivity with adaptive subchannelization and resource allocation, the OFDMA technique has gained much more interest in recent years. With transceiver PHN in OFDMA, CPE and in-band ICI are not the only sources of interference like OFDM but the multiplexing of several users introduces out-of-band interference from one user on another known as MUI [27].

## Acknowledgements

Acknowledgment is made to the Department of Electronics and Communication Engineering, BIET, and Editors, IntechOpen for the support to make this book chapter possible.

## Conflict of interest

The authors declare no conflict of interest.

## Notes/thanks/other declarations

Thanks to Prof. R. P. Yadav for his valuable suggestions and comments that helped to improve the presentation of the book chapter.

IntechOpen

IntechOpen

### **Author details**

Kamayani Shrivastav  
Bharat Institute of Engineering and Technology, Hyderabad, India

\*Address all correspondence to: 2014rec9012@mnit.ac.in

### **IntechOpen**

---

© 2022 The Author(s). Licensee IntechOpen. This chapter is distributed under the terms of the Creative Commons Attribution License (<http://creativecommons.org/licenses/by/3.0>), which permits unrestricted use, distribution, and reproduction in any medium, provided the original work is properly cited. 

## References

- [1] Cimini LJ. Analysis and simulation of a digital mobile channel using orthogonal frequency division multiplexing. *IEEE Transactions on Communications*. 1985; **COM-33**:665-675
- [2] Bingham JAC. Multicarrier modulation for data transmission: An idea whose time has come. *IEEE Communications Magazine*. 1990; **28**(5):5-14
- [3] Wu Y, Zou WY. Orthogonal frequency division multiplexing: A multi-carrier modulation scheme. *IEEE Transactions on Consumer Electronics*. 1995; **41**(3):392-399
- [4] Krondorf M, Fettweis G. OFDM link performance analysis under various receiver impairments. *EURASIP Journal on Wireless Communications and Networking*. 2008. DOI: 10.1155/2008/145279
- [5] Park MC, Han DS. Deep learning-based automatic modulation classification with blind OFDM parameter estimation. *IEEE Access*. 2021; **9**:108305-108317. DOI: 10.1109/ACCESS.2021.3102223
- [6] Robertson P, Kaiser S. Analysis of the effects of phase noise in orthogonal frequency division multiplex (OFDM) systems. In: *Proceedings of the IEEE ICC'95*. Seattle, WA; 1995. pp. 1652-1657
- [7] Armada A. Understanding the effects of phase noise in orthogonal frequency division multiplexing (OFDM). *IEEE Transactions on Broadcasting*. 2001; **47**(2):153-159
- [8] Wu S, Bar-Ness Y. OFDM systems in the presence of phase noise: Consequences and solutions. *IEEE Transactions on Communications*. 2004; **52**(11):1988-1997
- [9] Shrivastav K, Yadav RP, Jain KC. Cyclic gradient descent optimization for joint MAP estimation of channel and phase noise in OFDM. *IET Communications*. 2018; **12**(12): 1485-1490. DOI: 10.1049/iet-com.2017.0732
- [10] Mohammadian A, Tellambura C, Li GY. deep learning-based phase noise compensation in multicarrier systems. *IEEE Wireless Communications Letters*. 2021; **10**(10):2110-2114. DOI: 10.1109/LWC.2021.3093574
- [11] Demir A. Phase noise and timing jitter in oscillators with colored-noise sources. *IEEE Transactions on Circuits and Systems—I: Fundamental Theory and Applications*. 2002; **49**(12): 1782-1791
- [12] Hajimiri A, Lee T. A general theory of phase noise in electrical oscillators. *IEEE Journal of Solid-State Circuits*. 1998; **33**(2):179-194
- [13] Chorti A, Brookes M. A spectral model for RF oscillators with power-law phase noise. *IEEE Transactions on Circuits and Systems—I: Regular Papers*. 2006; **53**(9):1989-1999
- [14] Demir A. *Phase Noise in Oscillators: DAEs and Colored Noise Sources*. Bell Laboratories; 2011
- [15] Mathecken P, Riihonen T, Werner S, Wichman R. Performance analysis of OFDM with wiener phase noise and frequency selective fading channel. *IEEE Transactions on Communications*. 2011; **59**(5):1321
- [16] Ghosh AP, Qin W, Roitershtein A. Discrete-time Ornstein-Uhlenbeck process in a stationary dynamic environment. *Journal of Interdisciplinary mathematics*. 2016; **19**(1):1-35
- [17] Kamayani Shrivastav RP, Jain KC. Joint MAP detection for OFDM in

presence of phase noise from free running and phase locked loop oscillator. *Wireless Personal Communications*. 2019;**109**(6):563-577. DOI: 10.1007/s11277-019-06579-5

[18] Demir A, Mehrotra A, Roychowdhury J. Phase noise in oscillators: A unifying theory and numerical methods for characterization. *IEEE Transactions on Circuits Systems I, Fundamental, Theory & Applications*. 2000;**47**(5):655-674

[19] Ikeuchi K, Sakai M, Lin H. Compensation of phase noise in OFDM/OQAM systems. In: 2017 IEEE 86th Vehicular Technology Conference (VTC-Fall). 2017. pp. 1-5

[20] Shi Q, Wu N, Wang H, Nguyen DN, Huang X. Joint phase noise estimation and decoding in OFDM-IM. In: *GLOBECOM 2020 – 2020 IEEE Global Communications Conference*. 2020. pp. 1-6. DOI: 10.1109/GLOBECOM42002.2020.9348264

[21] Schlüter M, Dörpinghaus M, Fettweis GP. Joint phase and timing estimation with 1-bit quantization and oversampling. *IEEE Transactions on Communications*. 2022;**70**(1):71-86. DOI: 10.1109/TCOMM.2021.3113946

[22] Park CS, Gim Y, Park J, Park S. Design and implementation of a digital front-end with digital compensation for low-complexity 4G radio transceivers. *IEEE Access*. 2021;**9**:111432-111455. DOI: 10.1109/ACCESS.2021.3102949

[23] Kamayani Shrivastav RP, Jain KC. Joint MAP channel estimation and data detection for OFDM in presence of phase noise from free running and phase locked loop oscillator. *Digital Communications and Networks*. 2021;**7**(1):55-61. DOI: 10.1016/j.dcan.2020.09.007

[24] Srikanth S, Kumaran V, Manikandan C. Orthogonal frequency

division multiple access: Is it the multiple access system of the future? In: *AU-KBC Research*. India: Anna University; 2006

[25] Maeder A, Zein N. OFDMA in the field: Current and future challenges. *ACM SIGCOMM Computer Communication Review*. 2010;**40**(5): 71-76

[26] Shrivastav K, Yadav RP. Characterization of MUI for OFDMA uplink in presence of transceiver phase noise. *International Journal of Future Generation Communication and Networking*. 2017;**10**(6):23-32

[27] Mohammadian A, Tellambura C. Joint channel and phase noise estimation and data detection for GFDM. *IEEE Open Journal of the Communications Society*. 2021;**2**:915-933. DOI: 10.1109/OJCOMS.2021.3073348

# We are IntechOpen, the world's leading publisher of Open Access books Built by scientists, for scientists

6,300

Open access books available

171,000

International authors and editors

190M

Downloads

Our authors are among the

154

Countries delivered to

TOP 1%

most cited scientists

12.2%

Contributors from top 500 universities



WEB OF SCIENCE™

Selection of our books indexed in the Book Citation Index  
in Web of Science™ Core Collection (BKCI)

Interested in publishing with us?  
Contact [book.department@intechopen.com](mailto:book.department@intechopen.com)

Numbers displayed above are based on latest data collected.  
For more information visit [www.intechopen.com](http://www.intechopen.com)



# Multiplexing, Transmission and De-Multiplexing of OAM Modes through Specialty Fibers

*Alaaeddine Rjeb, Habib Fathallah and Mohsen Machhout*

## Abstract

Space division multiplexing (SDM) over fibers has introduced a new paradigm in optical communication thanks to its capability to meet the ever-renewed demand of more transmission capacity and on large spectral efficiency. This ever-increasing demand is pushed by the nonstop increase of the number of connected users, devices, processes, and data (toward internet of everything IOE). One of the most promising variants of SDM, that has recently shown great potential, is based on harnessing orbital angular momentum (OAM) modes as data carriers. These OAMs are multiplexed, transmitted over special optical fibers (OAM-fibers) then de-multiplexed. In order to highlight the potential of SDM system incorporating OAM modes through fibers, in this chapter, we disassemble an SDM system and we examine its main key elements. The potential of OAM-SDM is discussed as a promising candidate for the next generation local/global communications networks. This chapter is intended to provide a comprehensive and deep understanding of SDM, which will push R&D community to derive future research directions in the field.

**Keywords:** optical communication, space division multiplexing (SDM) systems, orbital angular momentum (OAM), optical fibers

## 1. Introduction

Over the last decade, there are unquestionably a huge demand for transmission capacity. This demand is fueling by the fast & renewed increase of the number of connected users, devices, processes, and data (e. g. According to the Annual Internet report of CISCO, there will be 5.3 billion total Internet users (66% of global population) by 2023, up from 3.9 billion (51% of global population) in 2018) [1]. This tend to create a hyper connected world. Furthermore, there are international efforts that aim to develop a concrete roadmap for “Internet Governance” targeting to both bring (i.e. to deliver) the internet to everyone (i.e. “connect the unconnected”) and provide enormous boost in performance of the actual Internet network. These efforts will put much pressure on the Internet service providers/communications actors and motivate them to reach innovative solutions and advanced technologies to deal with the growing insatiable on data capacity that will probably result in an imminent capacity crunch in the next few years [2]. On the other hand, optical fiber communication is still a milestone in the evolution of communication generally. Optical fiber is considered as the backbone of the modern

communications grid. Various research developments on optical fiber communication have been conducted showing great potential [3].

In order to cope with the huge demand of more and more data capacity, and improve the spectral efficiency, R&D optical fiber communication community has developed various technological paths based on innovative multiplexing techniques and advanced optical modulation formats. From one hand, various multiplexing techniques have been conducted based on the use of different optical signal dimensions as degrees of freedom to encode information and transmit them over optical fibers. These dimensions are the Time, as time division multiplexing (TDM: interleaving channels temporally), the polarization, Polarization division multiplexing (PDM), the wavelength, as wavelength division multiplexing (WDM: using multiple wavelength channels) and the phase (quadrature). These physical parameters help to create orthogonal signal sets even sharing the same medium (i.e. multiplexing); they do not interfere with each other (i.e. individual, separate and independent signals). **Figure 1** depicts these orthogonal dimensions. On the other hand, the improvement in modulation format is translated by the move on from the On-Off-Keying (OOK) modulation to M-ary Quadrature Amplitude Modulation (M-QAM), M-ary phase-shift keying (M-PSK) and M-ary amplitude-shift keying (M-ASK) [4–6].

Recently, researchers have oriented toward the space (Space Division Multiplexing (SDM)) as a further dimension to encode information [7]. The spatial analogue of the above cited dimensions, SDM is based on the exploitation of the spatial structure of the light (i.e. optical signal) or the spatial dimension of the physical transmission medium (e.g. optical fiber). Both strategies aim to improve the available data channels along an optical transmission link (i.e. Network). Considering these data channels, two attractive variants of SDM have shown potential interest: (1) Core Division Multiplexing (CDM) and (2) Mode Division Multiplexing (MDM). CDM is based on the increasing of the number of cores embedded in the same cladding of optical fiber [8]. These fibers are known as multicore fibers (MCFs). Other classical option that has been adopted in current optical infrastructure for several years already is based on single core fibers bundles (i.e. fibers are packed together creating a fiber bundle or

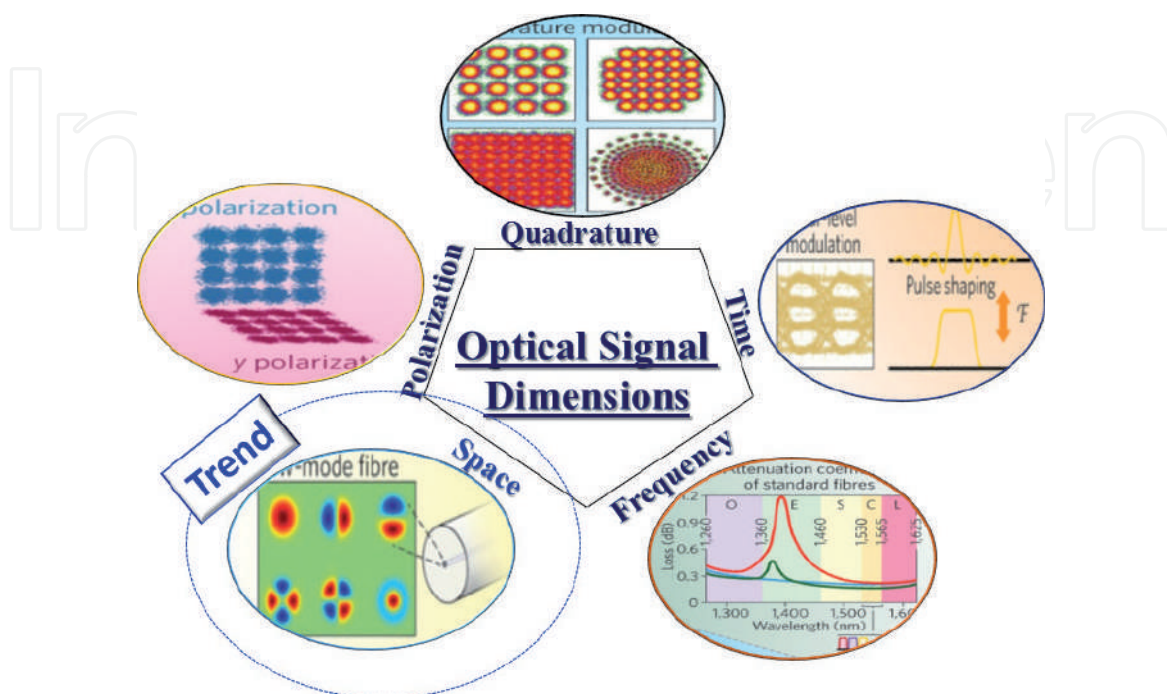


**Figure 1.**  
*Optical signal dimensions using as degrees of freedom to encode data.*

ribbon cable) [9]. If we assume that one core is equivalent to one data channel hence, the transmission capacity in an optical link incorporating MCFs will be multiplied by the number of embedded cores. On other side, MDM is consisting on the transmission of several spatial optical modes (various paths or trajectories) as data channels within common physical transmission medium (within the same core) targeting to boost the capacity transmission [10]. MDM could be realized by either multimode fibers (MMFs) or few mode fibers (FMFs). MMFs are dedicated to short transmission interconnect while FMFs are used for long haul transmission links. The same as CDM, if we assume that one mode is equivalent to one data channel; the transmission capacity in an optical link incorporating MMF/FMF will be multiplied by the number of supported modes. Other promising technology is based on mixing both approaches: Multicore few modes fibers (MC-FMF) where the number of channels will be proportional to the number of embedded cores and to the number of supported modes within the same core [11]. Moreover, MDM could be realized over free space link where data are carrying on multiple parallel laser beams that propagates over free space between transceivers [12].

Considering optical fiber links, numerous mode basis have been harnessed for mode division multiplexing showing its capability & effectiveness to scale up the capacity transmission and enhance the spectral efficiency. Recently, based on the feature that light can carry Angular Momentum (AM) (i.e. AM expresses the amount of dynamical rotation presents in the electromagnetic field representing the light), the capacity transmission of optical fiber has been unleashed [13]. The AM of a light beam is composed of two forms of momentums (i.e. rotation): (1) Spin Angular Momentum (SAM), which is related to the polarization of light (e.g. right or left circular polarization). SAM provide only two different states (available data channels). (2) Orbital Angular Momentum (OAM) which is linked to the spiral aspect (twisted light) of the wave front. This is related to a phase front of  $\exp(jl\varphi)$  where  $l$  is an arbitrary unlimited integer (theoretically) that indicates the degree of twist of a beam, and  $\varphi$  is the azimuthal angle [14]. Benefiting of two inherent features of OAM modes: first, two OAM modes with different topological charge  $l$  do not interfere (i.e. orthogonality). Second, the topological charge  $l$  is theoretically unlimited (i.e. unboundedness), exploiting the OAM of light as a further degree of freedom to encode information, is arguably one of the most promising approaches that has deserved a special attention over the last decade and showing promising achievements [15, 16]. OAM modes has been harnessed in multiplexing/de-multiplexing (OAM-SDM) or in increasing the overall optical channel capacity over optical fiber link. OAM-SDM is facing several key challenges, and lots crucial issues that it is of great importance to handle with it in order to truly realize the full potential of this promising technology and to paving the road to a robust and to a high capacity transmission operation with raised performances in next generation optical communication systems.

SDM is based on the orthogonality of spatial channels (spatial modes). Thus, mode coupling or mode mixing (e.g. channels crosstalk) is the main challenge in an SDM system and the main goals of that technology are in principle rotating around how to keep enough separation between much available modes. In order to cope with channel crosstalk, two solutions could be used. The first is the use of multiple input multiple output digital signal processing (MIMO DSP) [17] while the second is based on the optimization of fiber parameters (refractive index profile & fiber parameters) at the design stage [18]. In principle, MIMO DSP is considered as the extreme choice to decipher channels at the receiving stage since it is heavy and complex. This complexity is came from the direct proportionality between the number of required equalizer from one side and the transmission distance, the number of modes, and the difference between modes delays, from the other side. Hence, these

considering reasons allow the use of MIMO much impractical in real time and threats the scalability of optical communication SDM systems. Hence, by carefully manipulating the fiber design key parameters, it is possible to supervise/control the possible interactions between modes/channels. This better facilitates understanding each fiber parameter impact on fiber performances metrics and smooth the way of transition from the design stage to the fabrication process (e.g. MCVD as Modified Chemical Vapor Deposition) and to the deployment operation on the ground later (e.g. FTTH as Fiber To The Home and FTTX as Fiber To The x).

In this chapter, we detail the main key elements/actors (i.e. devices and parameters) that form an SDM system and allow it to become a promising approach to handle with the upcoming capacity crunch of the next generation optical communications systems. Then, we concentrate on the potential of using OAM modes over optical fibers (OAM-SDM) as a promising candidate that tend to realize the full potential for SDM technology. We provide the main generation, detection, transmission, challenges and future research directions of that technology. This aims to provide a comprehensive and deep understanding of OAM-SDM technology, which will push R&D community to derive future research directions in the field.

## 2. Space division multiplexing (SDM) system

In this section, we detail the optical fiber based SDM optical communication system. We describe essential devices/actors constructing a full SDM transmission line. We start by the emission side devices, then the SDM-fibers & amplifiers and at last the devices using for the reception of data at the receiver side. **Figure 2** illustrates a schematic representation of a generic SDM optical communication system.

### 2.1 Emission side

From the emission side, data ( $Data_i$ ) are modulated using for example a non-return to zero (NRZ) sequence. The electrical signal ( $ES_i$ ) converted into an optical signal using optical sources. These optical sources could be LED (light-emitting diode), DFB laser (distributed feedback laser), FP lasers (Fabry-Pérot laser diode), VCSEL (Vertical Cavity Surface Emitting Laser), etc. Each transmitter will couples the generated optical signal to a single mode fiber ( $SMF_i$ ) in order to excite the fundamental mode (i.e. namely  $LP_{01}$  mode) [19]. All the obtained modes are multiplexed using optical multiplexers (SDM MUX). SDM Optical multiplexers (also commonly called fan-in device) are spatial multiplexers that tend to collect modes (i.e. data carriers) from SMFs and couple them to an SDM fiber. For multiplexing various modes,

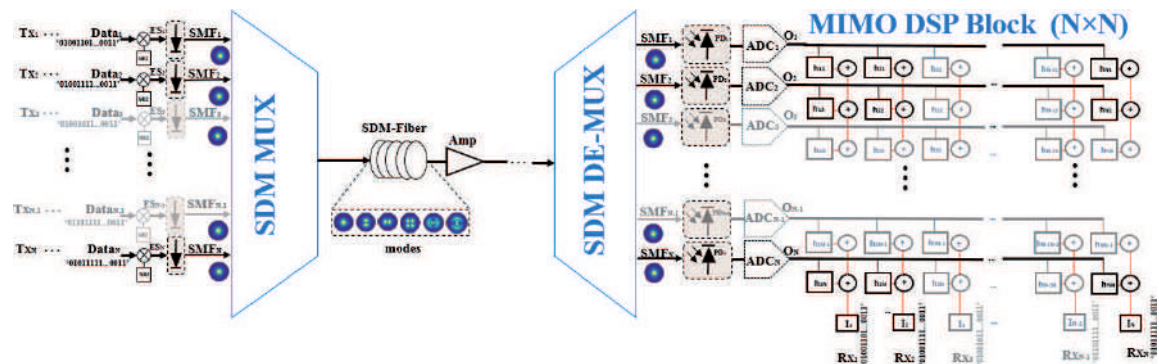


**Figure 2.** Schematic of a generic space division multiplexing system based on optical fiber communication.

several techniques and devices have been demonstration. Photonic lantern, Photonic integrated grating couplers waveguide optics interface, tapered multicore fibers, waveguide coupling (e.g. in case of MCFs, isolated waveguides connect each core to a particular SMF) and free space optics approaches such us phase plates, mirrors, beam splitters and special lenses [20]. In principle, the selection rule between these techniques are based on the incorporated SDM fiber (i.e. FMF, MMF MCF) and on the requirement of the lowest loss, the low susceptibility to crosstalk, the compactness, and low complexity and flexible.

## 2.2 SDM-optical fiber transmission

Various kinds of fibers are used for SDM communication systems. As indicated above, we divide them as CDM-fibers and MDM-fibers. Considering CDM, the first technology used as SDM fibers are based on the use of Single-core Fiber bundle (fiber ribbon) where parallels single mode fibers are packed together creating a fiber bundle or a ribbon cable. The overall diameter of these bundles varies from around 10–27 mm. Delivers up to hundreds of parallel links, fiber bundles have been commercially available [21, 22], and adopted in current optical infrastructure for several years already. Fiber ribbons are also commercially used in conjunction with several SDM transceiver technologies [23]. Another scheme is based on carrying data on single cores (single mode) embedded in the same fiber known as Multicore Fibers (MCF). Hence, each core is considered as an independent single channel. The most important constraint in MCFs is the inter-core crosstalk (XT) caused by signal power leakage from core to its adjacent cores that is controlled by core pitch (distance between adjacent cores denoted usually as  $\Lambda$ ) [24]. There are in Principle, two main categories of MCF: weakly coupled MCFs (=uncoupled MCF) and strongly coupled MCFs (=coupled MCF) depending on the value of coupling coefficient 'K' (used to characterize the crosstalk). Using the so-called supermodes to carry data, the crosstalk in coupled MCF must be mitigated by complex digital signal processing algorithms, such as multiple-input multiple-output digital signal processing (MIMO-DSP) techniques [25]. On the contrary, due to low XT in uncoupled MCF, it is not necessary to mitigate the XT impacts via complex MIMO, (see **Table 1**). In principle, three-crosstalk suppression schemes in uncoupled MCF could be incorporated, which are trench-assisted structure, heterogeneous core arrangement, and propagation-direction interleaving (PDI) technique [26].

The first paper on communication using MCF demonstrates a transmission of 112 Tb/s over 76.8 km in a 7-cores fiber using SDM and dense WDM in the C+L ITU-T bands. The spectral efficiency was of 14 b/s/Hz [27]. The second paper [28] shows an ultra-low crosstalk level ( $\leq -55$  dB over 17.6 km), which presents the lowest crosstalk between neighboring cores value to date. Other reported works, show high capacity (1.01 Pb/s) [29] over 52 km single span of 12-core MCF. In [30], over 7326 km, a record of 140.7 Tb/s capacity are reached. Considering MDM schemes, two types of fibers are dedicated to support that strategy. One is

	Weakly coupled MCFs	Strongly coupled MCFs
Coupling coefficient 'K' [ $m^{-1}$ ]	$K < 0.01$	$K > 0.1$
Core pitch ' $\Lambda$ ' [ $\mu m$ ]	$\Lambda > 30$	$\Lambda < 30$
MIMO DSP exigence	No need	Need

**Table 1.**  
*Classification and features of multicore fibers.*

based on the use of multimode fibers (MMF) while the second exploits the well-known few-mode fibers (FMF). The main difference between both is the number of modes (available channels). Since MMF can support large number of modes (tens), the intermodal crosstalk becomes large as well as the differential mode group delay (DMGD), where each mode has its own velocity, hence reducing the number of propagating modes along the fiber becomes viable solution. This supports FMF as a viable candidate for realizing SDM [31]. **Figure 3** recapitalizes examples of SDM optical fibers.

Due to the unavoidable attenuation over the transmission operation (i.e. degradation of the spatially multiplexed optical signals powers), SDM optical amplifiers are essential for a long-haul space division multiplexing (SDM) transmission system. Two requirements should be fulfilled by optical amplifiers, which are the large mode gain and the small difference between gains over different modes. In principle, two types of optical amplifiers, optical fiber amplifier OFA (e.g. erbium-doped fiber amplifier (EDFA [32]), fiber Raman amplifier (FRA)) and semiconductor optical amplifier SOA. Other approach is based on electro-optical repeaters or regenerators where the amplification process is performed in electronic regime [33]. A repeater is consisting of optical receiver (i.e. optical signal to electrical signal), amplifier and Optical transmitter (i.e. electrical signal to optical signal). Three functions could be conducted over the amplifier known as 1R, 2R, and 3R.

- 1R: re-amplification.
- 2R: re-amplification + re-shaping.
- 3R: re-amplification + re-shaping + re-timing.

### 2.3 Receiver side

After propagating over the fiber, an SDM-DE-MUX which tend to disengage propagating modes (sharing the same MCF or FMF) and oriented them to particular SMFs. In principle, SDM-DE-MUX devices or techniques are the same as SDM-MUX but in the inverse sense (known also as fan-out devices).

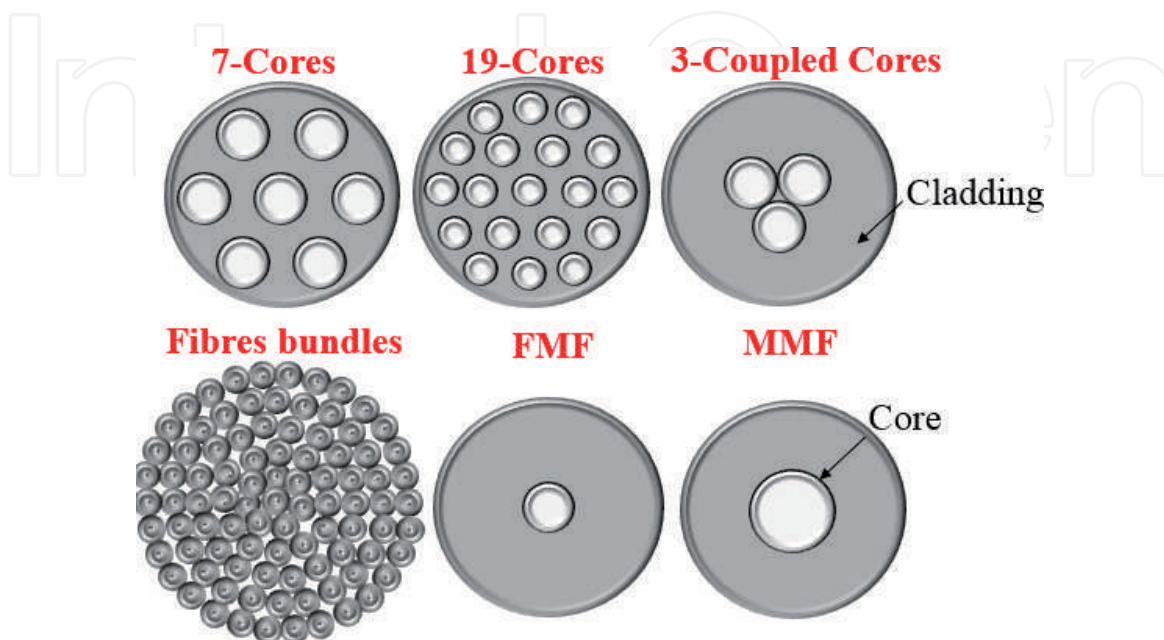


**Figure 3.**  
Several kinds of fibers used for SDM communication system.

After retrieving the optical signal (DE-MUX), optical photodectors are employed at the end of each SMF<sub>i</sub>, aiming to detect each particular mode (data carrier from each SMF<sub>i</sub>) and convert the modulated optical signal into an electrical signal. The most commonly used photodectors are semiconductor photodiodes. Semiconductor based PIN photodiode and the Avalanche photodiode (APDs) are examples of such photodectors. In principle, the selection of these devices is based on the following requirement: high responsivity, bandwidth, noise characteristics, low cost, and so on [34]. Thereafter, the obtained electrical signals are converted to digital ones using electrical-to-digital converters (ADCs). At the end, a MIMO DSP block is used to mitigate the crosstalk effects on different mode channels. The digital signal undergoes a normalizing/resampling and symbol synchronizing operations. Then, the obtained signals are equalized using adaptive time-domain equalization (TDE) or frequency-domain equalization (FDE). MIMO DSP are composed of equalizers (i.e. FIR filters) of coefficients  $h_{ij}$ . The number of these equalizers is related to the number of the square of the transmitted modes ( $N \times N$ ), the length of the transmission link, and the difference between modes delays [35, 36].

### 3. OAM-SDM system over fibers: potential and challenges

This section highlights the potential of carrying data on OAM modes and multiplexing, transmitting them over SDM fibers & de-multiplexing them. This technology is known as OAM-SDM technology. Intuitively, Incorporating OAM modes as data carriers has shown great potential in ameliorating the performances of SDM communication system. We focus on these OAM modes, what are they? How to generate and detect these kind of modes? What are the appropriate fibers that robustly support these modes? Moreover, what are the main challenges facing this technology?

#### 3.1 OAM beams

It is well known that an electromagnetic beam (light) possess angular momentum (AM), meaning that it can rotate around the propagation direction. Light possess a total AM of  $(l + s) \cdot \hbar$  per photon, where  $l\hbar$  corresponds to the orbital angular momentum (OAM) and  $s\hbar$  is the spin angular momentum (SAM) (see **Figure 4a**). The orbital angular momentum (OAM) beam, depends on the field spatial distribution, characterized by a helical phase front of  $\exp(il\phi)$ , where  $l$  denotes the topological charge number, which is an arbitrary integer ranging from  $-\infty$  to  $+\infty$ .  $\phi$  is the azimuthal angle, and  $\hbar$  is the reduced Planck constant ( $=1.055 \times 10^{-34}$  J s). The limitlessness of the topological charge number  $l$  indicates the unbounded states that can be modulated with OAM. In addition, two OAM lights with different  $l$  charge number are orthogonal. A series of wave fronts for various OAM modes are depicted in **Figure 4b**.

The sign of  $l$  denotes the handedness of the spiral. A clockwise rotation can be assigned to a positive  $l$  and an anticlockwise rotation to a negative  $l$ . On the other hand, the spin angular momentum (SAM) of light is related to the circular polarization state. The beam can only have bounded orthogonal states:  $S = \pm 1$ , which correspond to left or right circular polarization respectively. Intermediate values denote elliptical polarization. Benefiting by that inherent features (orthogonality & unbounded states), potential applications in diverse areas has exploited the OAM of light, including, but not limited to, optical trapping, tweezers, metrology, microscopy, imaging, optical speckle, astronomy, quantum entanglement, manipulation, and remote sensing (**Figure 5**) [13, 37–51]. As recent trend, Orbital

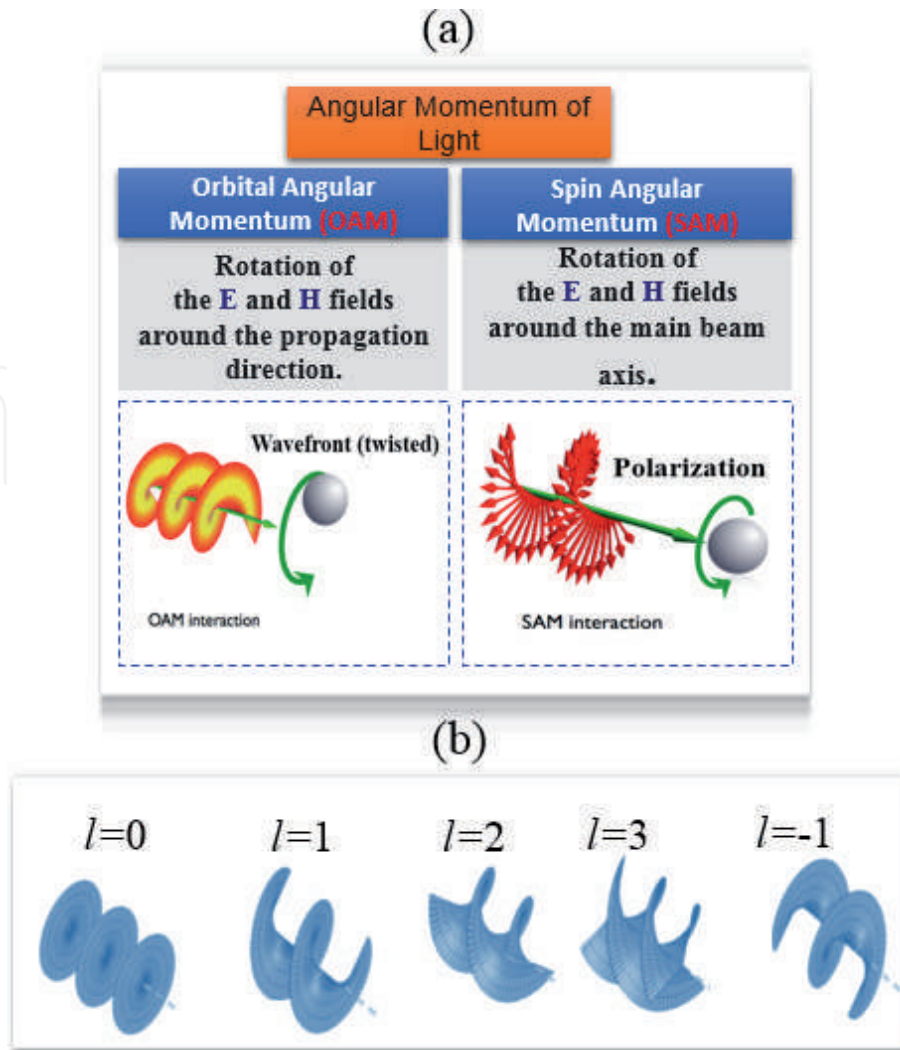


**Figure 4.** (a) The OAM and the SAM of an electromagnetic beam. (b) Helical wave fronts for a set of orbital angular momentum modes.

angular momentum (OAM) has gained a widespread interest in the area of optical telecommunication due to its capability to elevate the transmission capacity and substantially improve the spectral efficiency (OAM could offer unlimited channels for data transmission) of optical communication in both free space and fiber optics links. Many families of light beams can carry orbital angular momentum including Laguerre-Gaussian beams (LGB) [52], Bessel beams [53], Bessel-Gaussian beams (BGB) [54], Hermite-Gaussian beams (HGB) [55], Mathieu beams [56], Ince-Gaussian beams [57], and vector vortex beams [58].

### 3.2 Devices and components for OAM-SDM over fibers

In the original and the first experiment from Allen et al. in 1992 [52], helically phased LG beam was generated from Hermite-Gaussian (HG) beams. The transformation has been based on cylindrical lens (CL). The advantage of CL is its high conversion efficiency and the high purity of generated OAM. However, CL requires high construction precision. Indeed, it has poor flexibility because it requires a very precise incident field angle.

Other obvious way to implement OAM beams is to use a spiral phase plate (SPP) [59–64]. In principle, when a Gaussian light beam passes through the phase plate, the beam experiences a different phase in the azimuth direction due to the spiral

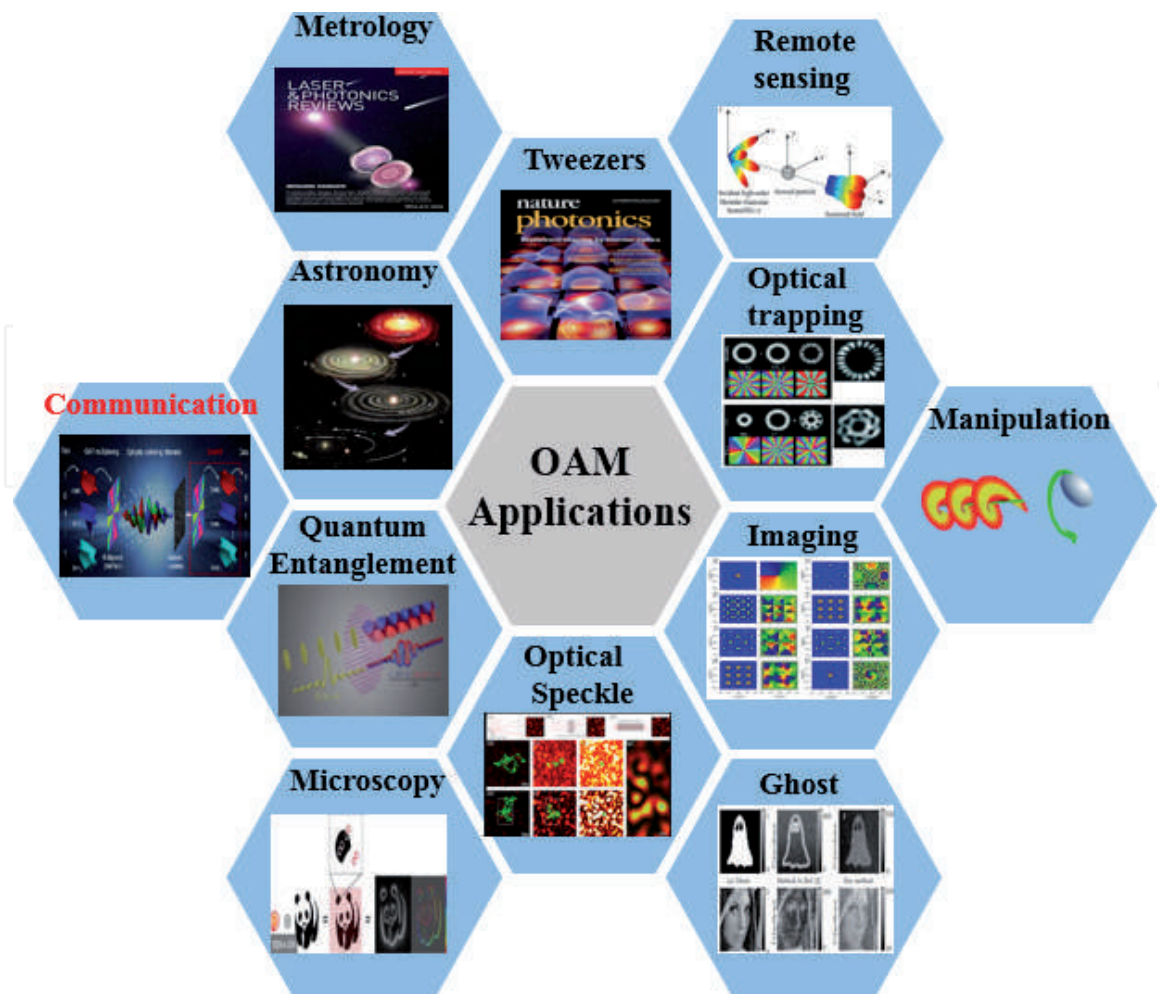


**Figure 5.**  
 Different applications of OAM.

thickness of the phase plate and is converted into a helically phased beam with topological charge  $l$ . The advantage of SPP is that is very efficient, and allows the conversion of beams with relatively high power. However, since it is wavelength dependent, it needs extreme precision in manufacturing: different plate is needed for each kind of OAM mode (each  $l$ ). Recent trend is the proposed adjustable spiral phase plate in [64]. Some diffractive optical devices or elements can be explored targeting to generate OAM light beams [65, 66]. Among these devices, fork grating are used for generating twisted light (holographic gratings). Fortunately, thanks to fork grating, we can generate multiple topological charges (different OAM beams) simultaneously (i.e. using vertical and horizontal superimposed fork gratings). However, this element seems to be inefficient and a variation of this technique has been proposed to improve its efficiency, using forked polarization grating [66]. Metamaterials (complex artificial materials) is another strategy that can make transformations in optical space [67, 68]. OAM modes are obtained by controlling the geometrical parameters (shape, size, direction, etc.) of the metamaterial to manipulate the phases of different azimuths and change the spatial phase of the incident light. A liquid crystal panel, q-plates is another promising and efficient way to generate twisted beams [69–71]. A light beam incident on q plate is modified to have a topological charge variation.

At last, one of the most convenient method to generate OAM beams is the use of spatial light modulator (SLM) [63, 72–74]. Made of liquid crystals, SLM is a programmable device that uses a computer [63]. It is composed of a matrix of pixels, and each pixel can be programmed to generate a given phase (there also exists SLMs

that act on amplitude instead of phase). By modulating the phases of Gaussian beams, we can generate a wide range of OAM modes. SLM is a versatile component, it can be reconfigured as needed. It is even possible to send different beams on different sections of the SLM, to generate several beams simultaneously. On the other hand, due to its polarization dependent, SLM accepts only limited power. Another method to generate OAM light beams, is possible to use optical fiber. Acting as a mode selector [75] or a mode converter [76, 77], optical fiber seems to be useful in OAM mode generation. Fiber coupler [78], mechanical grating [79, 80], tilted optical grating [81], helical grating [82], multicore fibers [83–86] and liquid core optical fiber [87] are example of such method. **Figure 6** presents the most of examples of OAM generation devices & schemes.

OAM beam is doughnut shaped (never has intensity at its center). This characteristic is not sufficient to identify OAM beams and their topological charge. At the receiver of a communication system, the different OAM modes can be separated easily by exploiting the orthogonality of the helical phase fronts. A variety of methods for detecting OAM has been proposed for light. In principle, the detection operation can be performed using several techniques including those used for the generation: The operation of OAM beams detection is similar to the generation but in the inverse sense (inverse SPP [88], holographic grating [51, 89]). A common way to identify OAM is to interfere (interference method) the incident beam with a Gaussian beam, and to visualize the resulting interference pattern on a camera. Two cases are resulted: If the incident beam is Gaussian, the interference pattern

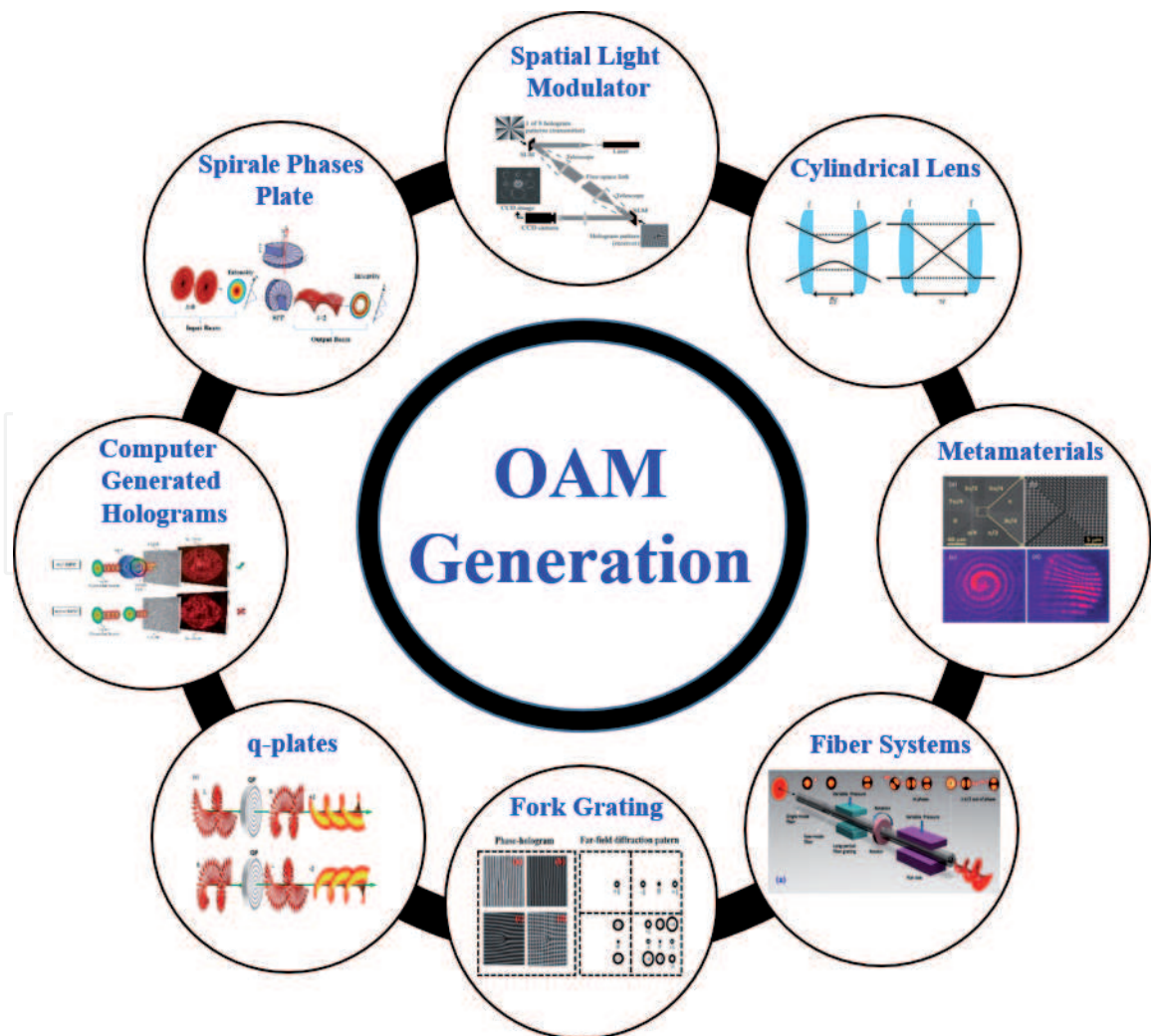


**Figure 6.**  
OAM generation devices & components & schemes.

will look like a series of concentric circles. If the incident beam has a helical phase front, the interference pattern will be a spiral. Then, the number of arms and the direction of the spiral indicate the topological charge and the sign of ' $l$ ' respectively. This technique is useful to validate the presence of OAM beam but it cannot be used for demultiplexing. Another efficient way, using a phase pattern or a fork grating on a glass plate or a SLM, to convert the incident beam back to Gaussian. A mode sorter was proposed to identify OAM modes, where the lateral position of the resulting beam tells the topological charge of the incident beam [90–92]. Recently, machine-learning-based approaches (ML) have been implemented in order to accurately identify OAM modes, after their propagation in free space [93, 94]. ML offer great potential in mode detection even after propagation in a turbulent medium. Many other OAM mode detection techniques are reviewed in [95, 96].

### 3.3 OAM-SDM-fibers: potentials and challenges

The utilization of OAM modes in optical fiber was a challenge to the optical communication community. This subsection focus on standard/special optical fibers designs that have been recently proposed investigated and incorporated in an OAM-SDM system. We start by the main designs and achievements and we will identify the main challenges that are facing this technology.

#### 3.3.1 OAM-SDM-fibers: potentials

Aiming to guide robust OAM modes over an optical fiber, scientists have oriented to special fiber design (i.e. novel refractive index profiles). In principle, these OAM-fibers share common three criteria:

- The refractive index profile should be ring (i.e. match the ring shape of OAM modes).
- The refractive indexes between core and cladding should be high (i.e. enhance the separation between channels).
- The interface between core and the cladding should be smooth (i.e. graded index profile is preferred).

Following these recommendations, various kinds of OAM-fibers have been proposed, characterized and prototyped showing potential achievements in term of capacity transmission and spectral efficiency. Moreover, the standard existing fibers have been investigating in term of their appropriateness to support OAM modes.

The investigation of already existing fibers in OAM context has been carried out by performing a comprehensive analysis of OAM modes in the standard graded index (GIF) multimode fiber (i.e. OM3) in [97]. The refractive index of GIF is shown in **Figure 6a**. Eventhough, the standard step index fiber (e.g. ITU-TG.652) is usually used as a single mode fiber (SIF); it is investigated as an OAM fiber by the utilization of small wavelengths (i.e. visible bands) which tend to change the former fiber to a few mode fiber (**Figure 6b**) [98]. Since then, the transmission of four-OAM mode groups over OM3 MMF, the transmission of OAM modes over OM4 (8.8 km) [99], the transmission of four OAM over 5 km FMF (i.e.  $4 \times 20$  Gbits/s QPSK data) [100], the high purity OAM modes ( $\geq 99.9\%$ ) over graded index FMF [101], and the viability of 12-OAM-GI-FMF for short/medium haul interconnect [102], have been demonstrated.

Considering the above design guidelines, specialty fibers have shown their capability to handle OAM modes. At the beginning, Ramachandran group has demonstrated the multiplexing/transmission and demultiplexing of OAM modes over a special vortex fiber [80]. The transmission of OAM modes over more than 20 m-VF [16] and 1 km-VF [103], have been demonstrated. Due to the high contrast between the air and the glass ( $\text{SiO}_2$ ) in term of refractive indexes, air core fibers (ACF) have been proposed, designed and prototyped (**Figure 6c**). An ACF supports 12 OAM modes over 2 m has been demonstrated in [104]. Two OAM modes supporting by an ACF was successfully transmitted over 1 km [105]. Another ACF fiber has been characterized in COPL at LAVAL University. This ACF supports 36 OAM states [106]. A capacity transmission of 10.56 Tbit/s has been demonstrated over an ACF using 12 OAM modes using WDM technology (OAM-SDM-WDM) [107]. Recently, over the O, E, S, C, and L bands, an ACF made by air,  $\text{As}_2\text{S}_3$  and  $\text{SiO}_2$  as material for the inner core, for the outer core and for the cladding, respectively, has been designed to support more than 1000 OAM modes [55, 108].

Ring core fibers RCF (**Figure 7d**) are another family of OAM specialty fibers that have been extensively investigated. COPL team has manufactured a family of RCFs suitable for OAM modes [109]. The transmission of two OAM mode-group has been demonstrated over a 50 km RCF [110]. Other RCF with smoothed refractive index at the interface between the core and the cladding, known as GIRCF, have been designed (**Figure 7e**). A GIRCF supporting 22 OAM modes over 10 km has been demonstrated [111]. An aggregate transmission capacity of 5.12 Tbits/s and a spectral efficiency of 9 bit/s/Hz have been reported in [112]. Over 12 km GIRCF, the transmission of two OAM modes each has 12 Gbaud (8QAM) and with 112 WDM channels has been demonstrated in [113]. Hence, a transmission capacity of 8.4 Tbits/s has been reported.

Other family of hybrid refractive index structure (i.e. inner core is graded while the outer core is step) have been proposed for OAM modes. Inverse parabolic graded

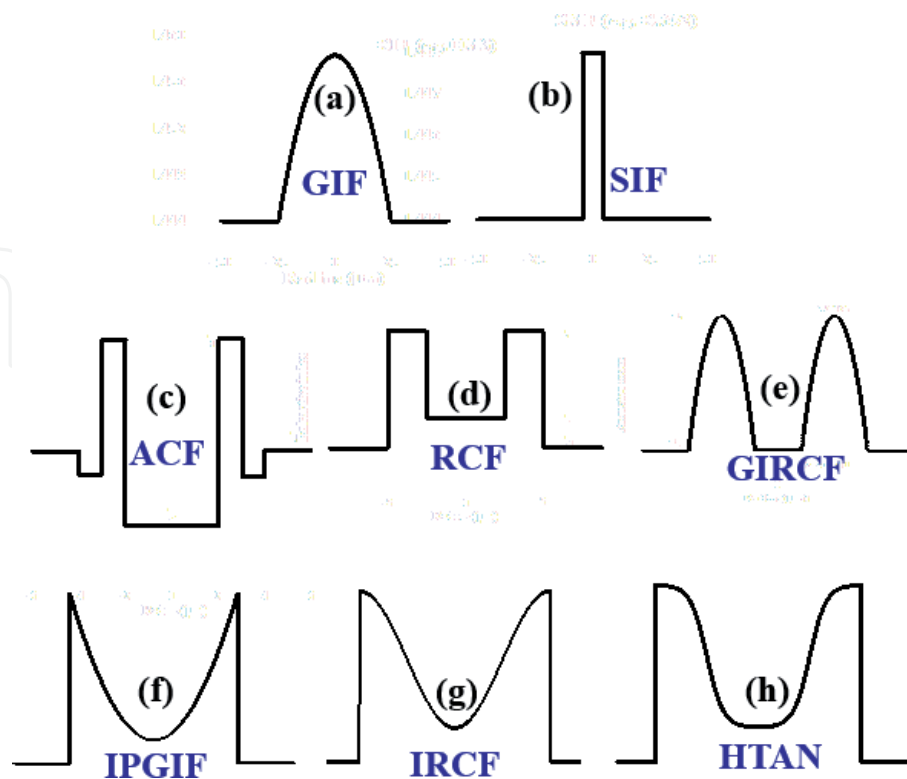


**Figure 7.** Various kinds of fibers that have been used in OAM-SDM systems: (a) graded index fiber, (b) step index fiber, (c) air core fiber, (d) ring core fiber, (e) graded index ring core fiber, (f) inverse parabolic graded index fiber, (g) inverse raised cosine fiber, (h) hyperbolic tangent fiber.

index fiber (IPGIF) has been designed and demonstrated experimentally (**Figure 7f**) [114]. As a first experiment, the use of IPGIF as OAM-fiber was successfully demonstrated based on the transmission of two OAM modes over 1 km. as a second step, 3.36 Tbits/s has been achieved over a IPGIF of 10 m. In that experiment, 15 wavelengths (WDM) and 4 OAM modes have been utilized [115]. In [116], we proposed inverse raised cosine fiber IRCF (**Figure 7g**) for supporting moderate and robust OAM modes. The new fiber proved the support of high pure OAM modes. Recently, we demonstrated the tolerance of IRCF in bend condition. Other usual function has been incorporated as a refractive index profile, which is the hyperbolic tangent function (HTAN). The designed fiber (**Figure 7h**) supports high pure OAM modes, with high separation among them (low crosstalk). The fiber is resilient to bending, and characterized by low chromatic dispersion and low differential group delay [117]. Recently, we designed an inverse-HTAN-MMF supporting very large number of OAM mode group (14 MG) that outperforms those supported by OM3 [118]. We designed another OAM-FMF based inverse Gaussian (IG) function. The designed IGF is favorable to transmit OAM modes in next generation OAM-MDM multiplexing optical networks [119].

The transmission of OAM modes over MCFs has been demonstrated with the aim of further increasing the capacity of an SDM links (i.e. improve the available data channels). A 7-RCF (MOMRF) has been proposed to support  $22 \times 7$  modes (i.e. 154 channels) [120]. Low-level crosstalk ( $-30$  dB) has been demonstrated over 100 km long MOMRF. A trenched multi OAM ring fiber (TA-MOMRF) has been reported in [121] showing Pbit/s as transmission capacity and hundreds bit/s/Hz as spectral efficiency. Later on, a coupled multi core fiber has been proposed in [122]. The investigated supermode fiber featured low crosstalk, low nonlinearity effects and low modal loss.

### 3.3.2 OAM-SDM-fibers: challenges

OAM-SDM over fibers is facing several key challenges and impediments that may curbs/slow down the transition from design process to prototyping operation and then to commercialization and standardization in the market.

Mode coupling issues are the most threads that degrade the OAM-SDM system performances. Mode coupling is the physical cause of data-channels crosstalk. Keeping these modes well separated during propagation along the fiber is a challenge in order to realize a robust OAM-SDM system and avoid the employment of additional MIMO-DSP module at the receiving stage. Even by using OAM-specialty fibers that ideally tend to appropriately support the OAM channels, there are almost some perturbations and impediments along the fiber section. These perturbations include macro & micro bending, twisting, birefringence, and core ellipticity. These imperfections may cause a mode coupling. Various linear and nonlinear effects in optical fiber could be detrimental for long distance SDM systems. Concerning linear effects, material absorption cause attenuation of optical signal (i.e. power loss). Other linear effects are the effects of dispersions during propagation. Chromatic dispersion is caused by the fact that the phase velocity and the group velocity are depending on the optical frequency. Polarization mode dispersions (PMD) are occurred because of dependency between the phase velocity of propagating mode and the polarization state. Intermodal dispersion is due to the dependency between the phase velocity and the optical mode.

On the other side, due to the intensity dependence of refractive index of optical fiber, and inelastic scattering phenomenon, different kind of nonlinearity effects can occur in optical fibers. This power material-light dependency is responsible for the Kerr-effect. Several effects are manifestations of Kerr nonlinearity. Four wave

mixing (parametric interaction among waves satisfying phases matching) arise when light components with different optical frequencies overlap in optical fiber. Stimulated Raman Scattering (SRS) is a nonlinear process that correspond to interaction between optical signals and molecular vibration in the glass-fiber (optical phonons). At last, stimulated Brillouin scattering (SBS) is very similar to Raman scattering that is correspond to interaction between optical signal and the acoustic vibration in the fiber (acoustic phonons).

#### **4. Perspectives and future research orientations**

Around a decade since the first OAM-SDM fiber, the ability of this technology has proven very fruitful in improving the optical communication networks in term of capacity, and spectral efficiency over long distances. However, it is still represent a young area of research and study that has a rich set of issues, challenges and opportunities to explore and to check it in the three regions of a communication link (emission, transmission, and reception). Starting by the emission side, important research directions are to find new materials and structures aiming to effectively generate OAM beams. These desired generation techniques or devices should feature favorable performances including low cost, high compactness, small size, high conversion efficiency, and compatibility with existing technologies. In addition, it would be important to give a significant interest in miniaturizing the devices and components at the emitter side (e.g. bringing OAM to the chip level in photonic circuits): Integrated on-chip devices on different platforms (e.g., silicon platform) could be viable candidates in next generation OAM SDM system. This helps OAM beams to be encoded & generated fast, switched freely and detected in real time. Various integrated version of devices could be widely adopted: integrated information encoders, integrated OAM modes emitters, and integrated OAM multiplexers. In spite of the price to be paid in term of cost, the development of such devices will be empowered by the rapid progress in micro and nano-fabrication technologies.

Considering optical fiber transmission phase, the perfect refractive index profile for OAM fiber is an open subject for everyone in optical communication. So far, it is unclear which kind of fiber provides the best performance in MDM, but evidently, there is no ideal OAM fiber design even if we either follow some design recommendations concluded from former proposed fibers (Section 3.3.1) or consider common electromagnetic rules. Certainly, each fiber has its pros and cons, but it is always a tradeoff between fiber key design parameters aiming to increase the number of supported modes, the separation among their refractive indexes, their purity, and their stability during transmission. Innovative designs with the former performances metrics would be an interesting direction of research. The desired designs will be motivated by the extended and the improvement of MOCVD process to support the manufacture of complex structure fibers with high refractive index contrast. Therefore, further efforts should be dedicated to develop new amplifiers. With the aim of further increasing the transmission capacity over long-haul optical fiber transmission systems, future R&D trends at the receiver side of SDM will based on the implementation of practical coherent optical communication schemes (coherent receivers) followed, if necessary, by advanced digital signal processing (DSP) techniques. It would be valuable in next generation OAM-SDM systems to explore techniques aiming to compensate both linear & nonlinear impairments (the compensation of nonlinear impairments is an interesting research area for coherent optical communications).

In addition, machine and Deep learning (ML & DL) have risen forefront in many fields. The use of ML or DL could touch various aspects from OAM-SDM

systems including nonlinearity mitigation, optical performance monitoring (OPM), carrier recovery, in-band optical signal-to-noise ratio (OSNR) estimation and modulation format classification, and especially, advanced DSP. Hence, a full smart optical communication networks.

## 5. Conclusions

Multiplexing spatial modes (SDM) seems to be viable solution to cope with the upcoming capacity crunch. In this chapter, we attempted to focus on the different aspects from an SDM system (emission, transmission and reception) over optical fibers aiming to highlight their main key elements and components that allow this technology to be the desired one for next generation local/global optical communication systems/networks. We focused on the last trend of SDM communication research direction: OAM-SDM over optical fibers. We discussed the OAM modes and the main devices & schemes for the generation & detection and the transmission of them. OAM specialty fibers are highlighted with focus on, their key features, their main achievements (throughput & main contributions) and main challenges that face their progress. Perspectives and future research orientations that may touching SDM systems have been presented at the end of this chapter. From what we have attempted to present, SDM still unexhausted research area that optical communication R&D community have to derive/touch future research directions in the field.

### Author details

Alaaeddine Rjeb<sup>1\*</sup>, Habib Fathallah<sup>2</sup> and Mohsen Machhout<sup>1</sup>

<sup>1</sup> Faculty of Sciences of Monastir, Laboratory of Electronic and Microelectronic, Physics Department, University of Monastir, Monastir, Tunisia

<sup>2</sup> Faculty of Sciences of Bizerte, Laboratory of Artificial Intelligence and Data Engineering Applications, Computer Department, University of Carthage, Bizerte, Tunisia

\*Address all correspondence to: [alaaeddine.rjeb@gmail.com](mailto:alaaeddine.rjeb@gmail.com)

### IntechOpen

© 2022 The Author(s). Licensee IntechOpen. This chapter is distributed under the terms of the Creative Commons Attribution License (<http://creativecommons.org/licenses/by/3.0>), which permits unrestricted use, distribution, and reproduction in any medium, provided the original work is properly cited. 

## References

- [1] Cisco VNI Global IP traffic forecast “2018-2023” Intelligence, Systems and Applications (IISA). IEEE; 2020. pp. 1-8
- [2] Chrallyvy A. Plenary paper: The coming capacity crunch. In: 2009 35th European Conference on Optical Communication. Austria Center Vienna, Austria: IEEE; 2009. pp. 1-1
- [3] Essiambre R, Tkach R. Capacity trends and limits of optical communication networks. *Proceedings of the IEEE*. 2012;**100**(5):1035-1055
- [4] Saridis GM, Alexandropoulos D, Zervas G, Simeonidou D. Survey and evaluation of space division multiplexing: From technologies to optical networks. *IEEE Communications Surveys & Tutorials*. 2015;**17**(4):2136-2156
- [5] Winzer PJ. Optical networking beyond WDM. *IEEE Photonics Journal*. 2012;**4**(2):647-651
- [6] Richardson DJ. Filling the light pipe. *Science*. 2010;**330**(6002):327-328
- [7] Richardson DJ, Fini JM, Nelson LE. Space-division multiplexing in optical fibres. *Nature Photonics*. 2013;**7**(5):354-362
- [8] Saitoh K, Matsuo S. Multicore fiber technology. *Journal of Lightwave Technology*. 2016;**34**(1):55-66
- [9] Sumitomo Electric [Online]. Available from: <http://www.sumitomoelectric.com/>
- [10] Yaman F, Bai N, Zhu B, Wang T, Li G. Long distance transmission in few-mode fibers. *Optics Express*. 2010;**18**(12):13250-13257
- [11] Papapavlou, Charalampos, Paximadis K, Tzimas G. Progress and demonstrations on space division multiplexing. In: 2020 11th International Conference on Information, Intelligence, Systems and Applications (IISA). IEEE; 2020. pp. 1-8
- [12] Willner AE, Liu C. Perspective on using multiple orbital-angular-momentum beams for enhanced capacity in free-space optical communication links. *Nano*. 2021;**10**(1):225-233
- [13] Yao AM, Padgett MJ. Orbital angular momentum: Origins, behavior and applications. *Advances in Optics and Photonics*. 2011;**3**(2):161-204
- [14] Rusch LA, Rad M, Allahverdyan K, Fazal I, Bernier E. Carrying data on the orbital angular momentum of light. *IEEE Communications Magazine*. 2018;**56**(2):219-224
- [15] Brning R, Ndagano B, McLaren M, Schrter S, Kobelke J, Duparr M, et al. Data transmission with twisted light through a free-space to fiber optical communication link. *Journal of Optics*. 2016;**18**:03LT01
- [16] Bozinovic N, Yue Y, Ren Y, Tur M, Kristensen P, Huang H, et al. Terabit-scale orbital angular momentum mode division multiplexing in fibers. *Science*. 2013;**340**(6140):1545-1548
- [17] Yang Z, Yu W, Peng G, Liu Y, Zhang L. Recent progress on novel DSP techniques for mode division multiplexing systems: A review. *Applied Sciences*. 2021;**11**(4):1363
- [18] Brunet C, Rusch LA. Optical fibers for the transmission of orbital angular momentum modes. *Optical Fiber Technology*. 2017;**35**:2-7
- [19] Klinkowski M, Lechowicz P, Walkowiak K. Survey of resource allocation schemes and algorithms in spectrally-spatially flexible optical networking. *Optical Switching and Networking*. 2018;**27**:58-78

- [20] Wartak MS. Computational Photonics: An Introduction with MATLAB. Cambridge University Press; 2013
- [21] Reflex Photonics [Online]. Available from: <http://www.reflexphotonics.com/>
- [22] OFS [Online]. Available from: <http://www.ofsoptics.com>
- [23] Samtec [Online]. Available from: <http://www.samtec.com>
- [24] Hayashi T, Taru T, Shimakawa O, Sasaki T, Sasaoka E. Design and fabrication of ultra-low crosstalk and low-loss multi-core fiber. *Optics Express*. 2011;**19**(17):16576-16592
- [25] Kingsta RM, Selvakumari RS. A review on coupled and uncoupled multicore fibers for future ultra-high capacity optical communication. *Optik*. 2019;**199**:163341
- [26] Ortiz AM, Sáez RL. Multi-core optical fibers: Theory, applications and opportunities. In: *Selected Topics on Optical Fiber Technologies and Applications*. IntechOpen; 2017
- [27] Zhu B, Taunay TF, Fishteyn M, Liu X, Chandrasekhar S, Yan MF, et al. 112-Tb/s space-division multiplexed DWDM transmission with 14-b/s/Hz aggregate spectral efficiency over a 76.8-km seven-core fiber. *Optics Express*. 2011;**19**(17):16665-16671
- [28] Hayashi T, Taru T, Shimakawa O, Sasaki T, Sasaoka E. Low-crosstalk and low-loss multi-core fiber utilizing fiber bend. In: *Optical Fiber Communication Conference/National Fiber Optic Engineers Conference 2011*. OSA Technical Digest (CD). Los Angeles, California United States: Optical Society of America; 2011. paper OWJ3
- [29] Takara H, Sano A, Kobayashi T, Kubota H, Kawakami H, Matsuura A, et al. T. 1.01-Pb/s (12 SDM/222 WDM/456 Gb/s) crosstalk-managed transmission with 91.4-b/s/Hz aggregate spectral efficiency. Presented at the European Conf. Exhibition Optical Communication. Amsterdam, The Netherlands. Paper Th.3.C.1. 2012
- [30] Igarashi K et al. 1.03-Exabit/s-km Super-Nyquist-WDM Transmission over 7,326-km Seven-Core Fiber. ECOC2013. PD1.E.3
- [31] Berdague S, Facq P. Mode division multiplexing in optical fibers. *Applied Optics*. 1982;**24**(11):1950-1955
- [32] Ono H, Yamada M, Takenaga K, Matsuo S, Abe Y, Shikama K, et al. Amplification method for crosstalk reduction in a multi-core fibre amplifier. *Electronics Letters*. 2013;**49**(2): 138-140
- [33] Simon, JC, Bramerie L, Ginovart F, Roncin V, Gay M, Fève S, et al. Chares ML. All-optical regeneration techniques. In: *Annales des télécommunications Vol. 58*(11). Springer-Verlag; 2003. pp. 1708-1724
- [34] Miyamoto Y, Takenouchi H. Dense space-division-multiplexing optical communications technology for petabit-per-second class transmission. *NTT Technical Review*. 2014;**12**(12):1-7
- [35] Zhao J, Liu Y, Xu T. Advanced DSP for coherent optical fiber communication. *Applied Sciences*. 2019;**9**(19):4192
- [36] Huang H, Milione G, Lavery MP, Xie G, Ren Y, Cao Y, et al. Mode division multiplexing using an orbital angular momentum mode sorter and MIMO-DSP over a graded-index few-mode optical fibre. *Scientific Reports*. 2015;**5**(1):1-7
- [37] Padgett M. Light's twist. *Proceedings of the Royal Society A: Mathematical, Physical and Engineering Sciences*. 2014;**470**(2172):20140633

- [38] Dennis MR, O'Holleran K, Padgett MJ. Singular optics: Optical vortices and polarization singularities. In: *Progress in Optics*. Vol. 53. Amsterdam: Elsevier; 2009. pp. 293-363. DOI: 10.1016/S0079-6638(08)00205-9
- [39] Ritsch-Marte M. Orbital angular momentum light in microscopy. *Philosophical Transactions of the Royal Society A: Mathematical, Physical and Engineering Sciences*. 2017;**375**(2087): 20150437
- [40] Padgett MJ. Orbital angular momentum 25 years on. *Optics Express*. 2017;**25**(10):11265-11274
- [41] Dholakia K, Čižmár T. Shaping the future of manipulation. *Nature Photonics*. 2011;**5**(6):335
- [42] Paterson L, MacDonald MP, Arlt J, Sibbett W, Bryant PE, Dholakia K. Controlled rotation of optically trapped microscopic particles. *Science*. 2001; **292**(5518):912-914
- [43] Padgett M, Bowman R. Tweezers with a twist. *Nature Photonics*. 2011;**5**(6):343-348
- [44] Simpson NB, Dholakia K, Allen L, Padgett MJ. Mechanical equivalence of spin and orbital angular momentum of light: An optical spanner. *Optics Letters*. 1997;**22**(1):52-54
- [45] Leach J, Dennis MR, Courtial J, Padgett MJ. Knotted threads of darkness. *Nature*. 2004;**432**(7014): 165-165
- [46] Dennis MR, King RP, Jack B, O'Holleran K, Padgett MJ. Isolated optical vortex knots. *Nature Physics*. 2010;**6**(2):118-121
- [47] Lavery MP, Speirits FC, Barnett SM, Padgett MJ. Detection of a spinning object using light's orbital angular momentum. *Science*. 2013;**341**(6145): 537-540
- [48] Giovannini D, Romero J, Potoček V, Ferenczi G, Speirits F, Barnett SM, et al. Spatially structured photons that travel in free space slower than the speed of light. *Science*. 2015;**347**(6224):857-860
- [49] Bernet S, Jesacher A, Fürhapter S, Maurer C, Ritsch-Marte M. Quantitative imaging of complex samples by spiral phase contrast microscopy. *Optics Express*. 2006;**14**(9):3792-3805
- [50] Elias NM. Photon orbital angular momentum in astronomy. *Astronomy & Astrophysics*. 2008;**492**(3):883-922
- [51] Mair A, Vaziri A, Weihs G, Zeilinger A. Entanglement of the orbital angular momentum states of photons. *Nature*. 2001;**412**(6844):313-316
- [52] Allen L, Beijersbergen MW, Spreeuw RJC, Woerdman JP. Orbital angular momentum of light and the transformation of Laguerre–Gaussian laser modes. *Physical Review A*. 1992;**45**:8185-8189
- [53] Gori F, Guattari G, Padovani C. Bessel–Gauss beams. *Optics Communication*. 1987;**64**:491-495
- [54] Ahmed N, Zhao Z, Li L, Huang H, Lavery MP, Liao P, et al. Mode-division-multiplexing of multiple Bessel-Gaussian beams carrying orbital-angular-momentum for obstruction-tolerant free-space optical and millimetre-wave communication links. *Scientific Reports*. 2016;**6**:22082
- [55] Ndagano B, Mphuthi N, Milione G, Forbes A. Comparing mode-crosstalk and mode-dependent loss of laterally displaced orbital angular momentum and Hermite–Gaussian modes for free-space optical communication. *Optics Letters*. 2017;**42**(20):4175-4178
- [56] Gutiérrez-Vega JC, Iturbe-Castillo MD, Chávez-Cerda S.

- Alternative formulation for invariant optical fields: Mathieu beams. *Optics Letters*. 2000;**25**:1493-1495
- [57] Bandres MA, Gutierrez-Vega JC. Ince–Gaussian beams. *Optics Letters*. 2004;**29**:144-146
- [58] Liu J, Chen X, He Y, Lu L, Ye H, Chai G, et al. Generation of arbitrary cylindrical vector vortex beams with cross-polarized modulation. *Results in Physics*. 2020;**19**:103455
- [59] Maurer C, Jesacher A, Furhapter S, Bernet S, Ritsch-Marte M. Tailoring of arbitrary optical vector beams. *New Journal of Physics*. 2007;**9**(3):78
- [60] Beijersbergen MW, Coerwinkel R, Kristensen M, Woerdman JP. Helical-wavefront laser beams produced with a spiral phaseplate. *Optics Communication*. 1994;**112**:321-327
- [61] Massari M, Ruffato G, Gintoli M, Ricci F, Romanato F. Fabrication and characterization of high-quality spiral phase plates for optical applications. *Applied Optics*. 2015;**54**:4077-4083
- [62] Turnbull GA, Roberson DA, Smith GM, Allen L, Padgett MJ. Generation of free-space Laguerre–Gaussian modes at millimetre-wave frequencies by use of a spiral phaseplate. *Optics Communication*. 1996;**127**:183-188
- [63] Oemrawsingh S, van Houwelingen J, Eliel E, Woerdman JP, Verstegen E, Kloosterboer J, et al. Production and characterization of spiral phase plates for optical wavelengths. *Applied Optics*. 2004;**43**:688-694
- [64] Sueda K, Miyaji G, Miyanaga N, Nakatsuka M. Laguerre-Gaussian beam generated with a multilevel spiral phase plate for high intensity laser pulses. *Optics Express*. 2004;**12**:3548-3553
- [65] Harm W, Bernet S, Ritsch-Marte M, Harder I, Lindlein N. Adjustable diffractive spiral phase plates. *Optics Express*. 2015;**23**(1):413-421
- [66] Gibson G, Courtial J, Padgett MJ, Vasnetsov M, Pas'ko V, Barnett SM, et al. Free-space information transfer using light beams carrying orbital angular momentum. *Optics Express*. 2004;**12**(22):5448-5456
- [67] Li Y, Kim J, Escuti MJ. Orbital angular momentum generation and mode transformation with high efficiency using forked polarization gratings. *Applied Optics*. 2012;**51**(34): 8236-8245
- [68] Zhao Z, Wang J, Li S, Willner AE. Metamaterials-based broadband generation of orbital angular momentum carrying vector beams. *Optics Letters*. 2013;**38**:932-934
- [69] Zeng J, Wang X, Sun J, Pandey A, Cartwright AN, Litchinitser NM. Manipulating complex light with metamaterials. *Scientific Reports*. 2013;**3**:2826
- [70] Marrucci L, Manzo C, Paparo D. Optical spin-to-orbital angular momentum conversion in inhomogeneous anisotropic media. *Physical Review Letters*. 2006; **96**:163905
- [71] Karimi E, Piccirillo B, Nagali E, Marrucci L, Santamato E. Efficient generation and sorting of orbital angular momentum eigenmodes of light by thermally tuned q-plates. *Applied Physics Letters*. 2009; **94**(23):231124
- [72] Lazarev G, Hermerschmidt A, Krüger S, Osten S. LCOS spatial light modulators: Trends and applications. In: Osten W, Reingand N, editors. *Optical Imaging and Metrology: Advanced Technologies*, chap. 1. Wiley-Blackwell; 2012. pp. 1-29
- [73] Heckenberg NR, McDuff R, Smith CP, White A. Generation of

optical phase singularities by computer-generated holograms. *Optics Letters*. 1992;**17**:221-223

[74] Ohtake Y, Ando T, Fukuchi N, Matsumoto N, Ito H, Hara T. Universal generation of higher-order multi ringed Laguerre-Gaussian beams by using a spatial light modulator. *Optics Letters*. 2007;**32**:1411-1413

[75] Cai X, Wang J, Strain MJ, Morris BJ, Zhu J, et al. Integrated compact optical vortex beam emitters. *Science*. 2012; **338**:363-366

[76] Volpe G, Petrov D. Generation of cylindrical vector beams with few-mode fibers excited by laguerre-gaussian beams. *Optics Communications*. 2004;**237**(1-3):89-95

[77] Witkowska A, Leon-Saval SG, Pham A, Birks TA. All-fiber lp<sub>11</sub> mode convertors. *Optics Letters*. 2008;**33**(4): 306-308

[78] Viswanathan NK, Inavalli VVG. Generation of optical vector beams using a two-mode fiber. *Optics Letters*. 2009;**34**(8):1189-1191

[79] Kumar R, Mehta DS, Sachdeva A, Garg A, Senthilkumaran P, Shakher C. Generation and detection of optical vortices using all fiber-optic system. *Optics Communications*. 2008;**281**(13):3414-3420

[80] Ramachandran S, Kristensen P, Yan MF. Generation and propagation of radially polarized beams in optical fibers. *Optics Letters*. 2009;**34**(16): 2525-2527

[81] Bozinovic N, Golowich S, Kristensen P, Ramachandran S. Control of orbital angular momentum of light with optical fibers. *Optics Letters*. 2012;**37**(13):2451-2453

[82] Fang L, Jia H, Zhou H, Liu B. Generation of cylindrically symmetric

modes and orbital-angular-momentum modes with tilted optical gratings inscribed in high-numerical-aperture fibers. *Journal of the Optical Society of America. A*. 2015;**32**(1):150-155

[83] Fang L, Wang J. Flexible generation/conversion/exchange of fiber-guided orbital angular momentum modes using helical gratings. *Optics Letters*. 2015;**40**(17):4010-4013

[84] Yan Y, Wang J, Zhang L, Yang J-Y, Fazal I, Ahmed N, et al. New approach for generating and (de)multiplexing oam modes in a fiber coupler consisting of a central ring and four external cores. In: 2011 37th European Conference and Exhibition on Optical Communication (ECOC). Geneva, Italy; 2011. pp. 1-3

[85] Yan Y, Wang J, Zhang L, Yang J-Y, Fazal IM, Ahmed N, et al. Fiber coupler for generating orbital angular momentum modes. *Optics Letters*. 2011;**36**(21):4269-4271

[86] Yan Y, Yang J-Y, Yue Y, Chitgarha MR, Huang H, Ahmed N, et al. High-purity generation and power-efficient multiplexing of optical orbital angular momentum (OAM) modes in a ring fiber for spatial-division multiplexing systems. In: Conference on Lasers and Electro-Optics 2012. San Jose, USA: Optical Society of America; 2012

[87] Yan Y, Yue Y, Huang H, Yang J-Y, Chitgarha MR, Ahmed N, et al. Efficient generation and multiplexing of optical orbital angular momentum modes in a ring fiber by using multiple coherent inputs. *Optics Letters*. Sep. 2012;**37**(17): 3645-3647

[88] Gao W, Hu X, Mu C, Sun P. Generation of vector vortex beams with a small core multimode liquid core optical fiber. *Optics Express*. May 2014;**22**(9):11 325-11 330

- [89] Willner AE, Huang H, Yan Y, Ren Y, Ahmed N, Xie G, et al. Optical communications using orbital angular momentum beams. *Advances in Optics Photonics*. 2015;7(1):66-106
- [90] Gao C, Zhang S, Fu S, Wang T. Integrating 5×5 dammann gratings to detect orbital angular momentum states of beams with the range of -24 to +24. *Applied Optics*. 2016;55(7):1514-1517
- [91] Berkhout GC, Lavery MP, Courtial J, Beijersbergen MW, Padgett MJ. Efficient sorting of orbital angular momentum states of light. *Physics Review Letters*. 2010;105(15):153601
- [92] Lavery MPJ, Robertson DJ, Berkhout GCG, Love GD, Padgett MJ, Courtial J. Refractive elements for the measurement of the orbital angular momentum of a single photon. *Optics Express*. 2012;20(3):2110-2115
- [93] Mirhosseini M, Malik M, Shi Z, Boyd RW. Efficient separation of the orbital angular momentum eigenstates of light. *Nature Communications*. 2013;4:2781
- [94] Doster T, Watnik AT. Machine learning approach to OAM beam demultiplexing via convolutional neural networks. *Applied Optics*. 2017;56:3386-3396
- [95] Park SR, Cattell L, Nichols JM, Watnik A, Doster T, Rohde GK. De-multiplexing vortex modes in optical communications using transport-based pattern recognition. *Optics Express*. 2018;26:4004-4022
- [96] Chen R, Zhou H, Moretti M, Wang X, Li J. Orbital angular momentum waves: Generation, detection and emerging applications. *IEEE Communications Surveys & Tutorials*. 2019;22(2):840-868
- [97] Chen S, Wang J. Theoretical analyses on orbital angular momentum modes in conventional graded-index multimode fibre. *Scientific Reports*. 2017;7(1):3990
- [98] Chen S, Wang J. Characterization of red/green/blue orbital angular momentum modes in conventional G.652 fiber. *IEEE Journal of Quantum Electronics*. 2017;53(4):1-14
- [99] Wang A, Zhu L, Wang L, Ai J, Chen S, Wang J. Directly using 8.8-km conventional multi-mode fiber for 6-mode orbital angular momentum multiplexing transmission. *Optics Express*. 2018;26(8):10038-10047
- [100] Wang A, Zhu L, Chen S, Du C, Mo Q, Wang J. Characterization of LDPC-coded orbital angular momentum modes transmission and multiplexing over a 50-km fiber. *Optics Express*. 2016;24(11):11716-11726
- [101] Zhang Z, Gan J, Heng X, Wu Y, Li Q, Qian Q, et al. Optical fiber design with orbital angular momentum light purity higher than 99.9%. *Optics Express*. 2015;23(23):29331-29341
- [102] Rjeb A, Seleem H, Fathallah H, Machhout M. Design of 12 OAM-Graded index few mode fibers for next generation short haul interconnect transmission. *Optical Fiber Technology*. 2020;55:102148
- [103] Bozinovic N, Ramachandran S, Brodsky M, Kristensen P. Record-length transmission of entangled photons with orbital angular momentum (vortices). In: *Frontiers in Optics*. Rochester, NY: Optical Society of America; 2011. p. PDPB1
- [104] Gregg P, Kristensen P, Golowich S, Olsen J, Steinvurzel P, Ramachandran S. Stable transmission of 12 OAM states in air-core fiber. In: *CLEO*. San Jose, California: Optical Society of America; 2013
- [105] Gregg P, Kristensen P, Ramachandran S. OAM stability in fiber

due to angular momentum conservation. In: CLEO. San Jose, California: Optical Society of America; 2014. p. 2014

[106] Brunet C, Vaity P, Messaddeq Y, LaRochelle S, Rusch LA. Design, fabrication and validation of an OAM fiber supporting 36 states. *Optics Express*. 2014;22(21):26117-26127

[107] Ingerslev K, Gregg P, Galili M, Da Ros F, Hu H, Bao F, et al. 12 mode, WDM, MIMO-free orbital angular momentum transmission. *Optics Express*. 2018;26:20225-20232

[108] Wang Y, Bao C, Geng W, Lu Y, Fang Y, Mao B, et al. Air-core ring fiber with >1000 radially fundamental OAM modes across O, E, S, C, and L bands. *IEEE Access*. 2020;8:68280-68287

[109] Brunet C, Ung B, Wang L, Messaddeq Y, LaRochelle S, Rusch LA. Design of a family of ring-core fibres for OAM transmission studies. *Optics Express*. 2015;23(8):10553-10563

[110] Zhang R, Tan H, Zhang J, Shen L, Liu J, Liu Y, et al. A novel ring-core fiber supporting MIMO-free 50 km transmission over high-order OAM modes. In: Proc. Opt. Fiber Commun. Conf. (OFC). California United States: Optical Society of America; 2019. pp. 1-3

[111] Zhu G, Chen Y, Du C, Zhang Y, Liu J, Yu S. A graded index ring-core fiber supporting 22 OAM states. In: Opto-Electronics and Communications Conference (OECC) and Photonics Global Conference (PGC). Singapore: IEEE; 2017. pp. 1-3

[112] Zhu G et al. Scalable mode division multiplexed transmission over a 10-km ring-core fiber using high-order orbital angular momentum modes. *Optics Express*. 2018;26:594-604

[113] Zhu L, Zhu G, Wang A, Wang L, Ai J, Chen S, et al. 18 km low-crosstalk

OAM+WDM transmission with 224 individual channels enabled by a ring-core fiber with large high-order mode group separation. *Optics Letters*. 2018;43(8):1890-1893

[114] Ung P, Vaity L, Wang Y, Messaddeq LA, LaRochelle RS. Few-mode fiber with inverse-parabolic graded-index profile for transmission of OAM-carrying modes. *Optics Express*. 2014;22(15):18044-18055

[115] Wang X, Yan S, Zhu J, Ou Y, Hu Z, Messaddeq Y, et al. 3.36-tbit/s oam and wavelength multiplexed transmission over an inverse-parabolic graded index fiber. In: 2017 Conference on Lasers and Electro-Optics (CLEO). IEEE; 2017. pp. 1-2

[116] Rjeb A, Guerra G, Issa K, Fathallah H, Chebaane S, Machhout M, et al. *Optics Communications*. 2020; 458:124736

[117] Rjeb A, Fathallah H, Khaled I, Machhout M, Alshebeili SA. A novel hyperbolic tangent profile for optical fiber for next generation OAM-MDM systems. *IEEE Access*. 2020; 8:226737-226753

[118] Rjeb A, Seleem H, Fathallah H, Machhout M. A novel inverse gaussian profile for orbital angular momentum mode division multiplexing optical networks. In: 2021 18th International Multi-Conference on Systems, Signals & Devices (SSD). Monastir, Tunisia: IEEE; 2021. pp. 480-487

[119] Rjeb A, Fathallah H, Issa K, Machhout M, Alshebeili SA. Inverse hyperbolic tangent fiber for OAM mode/mode-group division multiplexing optical networks. *IEEE Journal of Quantum Electronics*. 2021;57(4):1-12. DOI: 10.1109/JQE.2021.3090993.

[120] Li S, Wang J. Multi-orbital-angular-momentum multi-ring fiber for high-density space-division

multiplexing. *IEEE Photonics Journal*.  
2013;5(5):7101007-7101007

[121] Li S, Wang J. A compact trench-assisted multi-orbital-angular-momentum multi-ring fiber for ultrahigh-density space-division multiplexing (19 rings × 22 modes). *Scientific Reports*. 2014;4:3853

[122] Li S, Wang J. Supermode fiber for orbital angular momentum (OAM) transmission. *Optics Express*. 2015;23:18736-18745

IntechOpen